

EXTREMELY INEFFICIENT STAR FORMATION IN THE OUTER DISKS OF NEARBY GALAXIES

F. BIGIEL^{1,2}, A. LEROY^{2,3,7}, F. WALTER², L. BLITZ¹, E. BRINKS⁴, W. J. G. DE BLOK⁵, B. MADORE⁶

Accepted for Publication in the Astronomical Journal

ABSTRACT

We combine data from The H I Nearby Galaxy Survey and the GALEX Nearby Galaxy Survey to study the relationship between atomic hydrogen (H I) and far-ultraviolet (FUV) emission outside the optical radius (r_{25}) in 17 spiral and 5 dwarf galaxies. In this regime, H I is likely to represent most of the ISM and FUV emission to trace recent star formation with little bias due to extinction, so that the two quantities closely trace the underlying relationship between gas and star formation rate (SFR). The azimuthally averaged H I and FUV intensities both decline with increasing radius in this regime, with the scale length of the FUV profile typically half that of the H I profile. Despite the mismatch in profiles, there is a significant spatial correlation (at 15'' resolution) between local FUV and H I intensities; near r_{25} this correlation is quite strong, in fact stronger than anywhere inside r_{25} (where H I is not a good tracer for the bulk of the ISM), and shows a decline towards larger radii. The star formation efficiency (SFE) — defined as the ratio of FUV/H I and thus the inverse of the gas depletion time — decreases with galactocentric radius across the outer disks, though much shallower than across the optical disks. On average, we find the gas depletion times to be well above a Hubble time ($\sim 10^{11}$ yr). We observe a clear relationship between FUV/H I and H I column in the outer disks, with the SFE increasing with increasing H I column. Despite observing systematic variations in FUV/H I, we find no clear evidence for step-function type star formation thresholds, though we emphasize that it may not be realistic to expect them. When compared with results from inside r_{25} , we find outer disk star formation to be distinct in several ways: it is extremely inefficient (depletion times of many Hubble times which are also long compared to either the free fall or orbital timescale) with column densities and SFRs lower than found anywhere inside the optical disks. It appears that the H I column is one of, perhaps even the key environmental factor in setting the SFR in outer galaxy disks.

Subject headings: galaxies: evolution — galaxies: ISM — radio lines: galaxies — stars: formation

1. INTRODUCTION

When galaxies are observed with sufficient sensitivity, star formation is often seen to extend well beyond the optical disks, reaching far into the extended H I disks. After early indications of extended UV emission in nearby galaxies (e.g., Donas et al. 1981), the discovery of extended UV (XUV) disks in a large number of nearby galaxies was one of the major achievements of the GALEX mission (Thilker et al. 2005; Gil de Paz et al. 2005; Thilker et al. 2007; Gil de Paz et al. 2007b; Boissier et al. 2007; Zaritsky & Christlein 2007; Thilker et al. 2009; Hunter et al. 2010). Extended star formation is seen not only in the UV, but also in the optical, e.g., in deep H α and broad band observations, which reveal populations of young stars in the outer disks (Ferguson et al. 1998; Lelièvre & Roy 2000; Cuillandre et al. 2001; de Blok & Walter 2003;

Christlein & Zaritsky 2008; Herbert-Fort et al. 2010; Goddard et al. 2010; Werk et al. 2010). This agrees well with the observations that indirect tracers of past or likely future star formation, like dust (Zaritsky 1994; Popescu & Tuffs 2003; Dong et al. 2008), CO emission (Braine & Herpin 2004; Braine et al. 2007; Gardan et al. 2007), and metals (Gil de Paz et al. 2007b; Bresolin et al. 2009), are detected in the extended H I envelopes of galaxies.

Star formation at large radii usually does not account for a large fraction of a galaxy's total star formation rate (SFR), but studying this process offers a way to illuminate the physics behind the star formation process (e.g., Bush et al. 2008, 2010): low metallicities and dust abundances, relatively high shear, low total gas column densities spread over significant scale heights, a preponderance of H I compared to H₂, and a comparatively weak stellar potential well make the ISM in outer galaxy disks a distinctly different environment compared to the typical star-forming ISM in the inner part of a galaxy. This contrast leads to a much lower rate of star formation per unit gas mass at large galactocentric radii and to the conclusion that the physics behind the conversion of gas into stars *must be* affected by these environmental factors (e.g., Leroy et al. 2008).

A robust, quantitative picture of how the environment in outer disks affects star formation is important if we want to understand the origins of galaxy structure. Star formation at large galactocentric radii will affect how chemical enrichment varies across a galaxy

¹ Department of Astronomy, Radio Astronomy Laboratory, University of California, Berkeley, CA 94720, USA; bigiel@astro.berkeley.edu

² Max-Planck-Institut für Astronomie, Königstuhl 17, 69117 Heidelberg, Germany

³ National Radio Astronomy Observatory, 520 Edgemont Road, Charlottesville, VA 22903, USA

⁴ Centre for Astrophysics Research, University of Hertfordshire, Hatfield AL10 9AB, UK

⁵ Department of Astronomy, University of Cape Town, Rondebosch 7701, South Africa

⁶ Observatories of the Carnegie Institution of Washington, Pasadena, CA 91101, USA

⁷ Hubble Fellow

(Gil de Paz et al. 2007b) and plays a critical role in determining the location and form of the break in the exponential stellar disk (Pohlen & Trujillo 2006). Also, many galaxies sustain a large reservoir of (low column density) gas in their outer disks over evolutionary time scales. Measuring the gas consumption time scale in this regime for many galaxies and comparing it to the gas consumption time found for the inner parts of galaxies may provide valuable clues regarding the role of outer disk gas for fueling star formation over cosmological times (e.g., Shlosman, Frank & Begelman 1989; Blitz 1996; Bauermeister et al. 2009).

In this paper, we study the relationship between atomic gas (H I) and star formation at large galactocentric radii. We use state-of-the-art H I (‘The H I Nearby Galaxy Survey’, THINGS, Walter et al. 2008) and UV data (‘GALEX Nearby Galaxy Survey’, NGS, Gil de Paz et al. 2007a), which provide the field-of-view and the sensitivity needed to probe into the outer disks of galaxies while still offering the resolution to examine the interplay between gas (H I) and star formation locally, i.e., on scales of a few times 100 pc.

We use these two datasets to study the relationship between H I and star formation in 22 outer galaxy disks (defined as $r = 1-2 \times r_{25}$). We assess whether the observed decline of the SFR with galactocentric radius is predominantly due to a decreasing gas supply and we look for signs of star formation thresholds, as suggested theoretically and by observations of sharp truncations in radial distributions of H II regions (e.g., Martin & Kennicutt 2001). We examine radial and local variations in the star formation efficiency (SFE), i.e., the SFR normalized to the H I column (and thus the inverse of the gas consumption time) and variations in the spatial correlation of star formation and H I with galactocentric radius. We compare our results for the outer disks of spirals to dwarf galaxies (which share many of the same environmental factors) and link them to observations from within the optical disks of an overlapping set of galaxies (Bigiel et al. 2008; Leroy et al. 2008).

2. DATA

We study 22 galaxies: 17 spiral and 5 dwarf galaxies. This sample is constructed from the overlap of THINGS (Walter et al. 2008) and targets of the GALEX NGS (Gil de Paz et al. 2007a) that were observed to similar depth (integration time of $\gtrsim 1.5$ ks, corresponding to at least one orbit, which is the standard integration time for GALEX NGS targets). Table 1 lists our sample along with adopted distance, inclination, position angle, optical radius r_{25} and morphology (from Walter et al. 2008, except that we adopt $i = 20^\circ$ in NGC 5194). We correct all maps for inclination using the angles given in Table 1.

To allow a rigorous comparison, we degrade all H I and UV maps to a common resolution of $15''$ (set by the H I map with the lowest resolution) by convolving with a circular Gaussian beam. We have carried out a parallel analysis at a matched physical resolution of 1 kpc (set by the largest physical resolution in our sample) and find that for the spirals our results for the two cases differ only marginally. For the five dwarfs in our sample, working at 1 kpc resolution significantly reduces the number of independent measurements (per galaxy and total), constrain-

ing our ability to robustly compare the two approaches due to the limited statistics. In the following we thus only present the matched angular resolution case. The average physical resolution in our sample is ~ 600 pc, varying between ~ 230 pc and ~ 1 kpc across the sample.

We focus on the outer disks of galaxies, which we defined to be between 1 and $2 \times r_{25}$, where r_{25} is the isophotal radius corresponding to 25 B-band magnitudes per square arcsecond. This regime is illustrated in Figure 1 for one galaxy, NGC 3621. The left panel shows the THINGS H I and the right panel the GALEX far UV map. The overplotted annuli indicate 1 and $2 \times r_{25}$ in the plane of the galaxy, respectively.

2.1. A Note on Terminology

Throughout this paper we compare 21-cm intensity to far UV intensity. We will refer to 21-cm intensity and the surface densities of both H I and ‘gas’ interchangeably because we consider it likely that opacity effects in the 21-cm line and the contribution of molecular gas are both small in the regime we study. Similarly, we measure far UV intensities, I_{FUV} , from the GALEX maps. We convert these intensities into an approximate SFR surface density (Σ_{SFR}) using the assumptions discussed below (§ 2.4) and will use the terms ‘UV intensity’ and ‘star formation rate surface density’ to mean the same thing (I_{FUV}). In both cases, the reader interested in linking our plots directly to observables has only to make a linear transformation of any axis using the equations given in this paper.

When we refer to the conversion of H I into stars we implicitly assume that the gas becomes molecular first, i.e., H I forms into H_2 which then forms stars. Because H_2 in outer disks is not readily observable, we are forced to consider a ‘zoomed-out’ version of this process, the conversion of H I into stars with H_2 as an unconstrained intermediate phase. H_2 likely constitutes only a small fraction of the gas mass in outer disks, so the question of what drives the ISM to form stars in outer disks may still be robustly addressed using only H I and FUV.

There is no set of wide-field CO maps that extends to $2r_{25}$ (the widest-field maps reach $\sim r_{25}$, Leroy et al. 2009). However, we can readily see that from the (averaged) star formation rate surface densities that we infer for outer disks ($\Sigma_{\text{SFR}} \approx 10^{-6} - 10^{-4} \text{ M}_\odot \text{ yr}^{-1} \text{ kpc}^{-2}$, see § 3) that CO is likely to be very faint and H_2 is only a relatively minor part of the ISM. If these Σ_{SFR} were found in the disk of a spiral galaxy, the corresponding H_2 surface densities would be $\Sigma_{\text{H}_2} \sim 0.01 - 1 \text{ M}_\odot \text{ pc}^{-2}$ (Bigiel et al. 2008), roughly corresponding to a single giant molecular cloud ($M_{\text{H}_2} \approx 10^4 - 10^6 \text{ M}_\odot$) per resolution element. This is low enough to assume that H I comfortably dominates the ISM across our data on (approximately) kpc scales and implies CO intensities well below the detection limits of most existing maps. Because of this negligible contribution of H_2 to the gas budget and the lack of CO observations, we are confident using H I emission to trace the bulk distribution of the mass in the ISM in outer disks on kpc scales.

Readers interested in comparing this paper to other results should also note that we neglect any contribution from helium or heavier elements when quoting gas sur-

TABLE 1
SAMPLE PROPERTIES¹

Galaxy	D [Mpc]	i [deg]	PA [deg]	r_{25} [arcmin]	r_{25} [kpc]	Hubble type
Dwarfs						
DDO 154	4.3	66	230	1.0	1.2	Irr
Ho I	3.8	12	50	1.7	1.8	Irr
Ho II	3.4	41	177	3.3	3.3	Irr
IC 2574	4.0	53	56	6.4	7.5	SABm
NGC 2366	3.4	64	40	2.2	2.2	Irr
Spirals						
NGC 0628	7.3	7	20	4.9	10.4	Sc
NGC 0925	9.2	66	287	5.4	14.3	Scd
NGC 2403	3.2	63	124	7.9	7.4	SABc
NGC 2841	14.1	74	153	3.5	14.2	Sb
NGC 2903	8.9	65	204	5.9	15.2	SABb
NGC 3198	13.8	72	215	3.2	13.0	Sc
NGC 3351	10.1	41	192	3.6	10.6	Sb
NGC 3521	10.7	73	340	4.2	12.9	SABb
NGC 3621	6.6	65	345	4.9	9.4	SBcd
NGC 3627	9.3	62	173	5.1	13.8	SABb
NGC 4736	4.7	41	296	3.9	5.3	Sab
NGC 5055	10.1	59	102	5.9	17.3	Sbc
NGC 5194	8.0	20	172	3.9	9.0	Sbc
NGC 5236	4.5	24	225	7.7	10.1	Sc
NGC 5457	7.4	18	39	12.0	25.8	SABc
NGC 7331	14.7	76	168	4.6	19.5	Sbc
NGC 7793	3.9	50	290	5.2	5.9	Scd

¹ See Walter et al. (2008) for further information on individual galaxies and for references to the values quoted in this table.

face densities, but that we do take them into account when quoting star formation efficiencies or gas depletion times.

2.2. THINGS H I

To estimate the surface density of neutral, atomic hydrogen, Σ_{HI} , we use VLA maps of the 21-cm line obtained as part of ‘The H I Nearby Galaxy Survey’ (THINGS, Walter et al. 2008). THINGS consists of high-resolution, high-sensitivity H I data for 34 nearby galaxies obtained with the NRAO⁸ VLA. We use ‘natural’ weighted maps, which offer the best possible signal-to-noise ratios and have an average synthesized beam size of $\sim 11''$. These maps are sensitive ($\sim 3\sigma$) to column densities of $\Sigma_{\text{HI}} \gtrsim 0.4 \text{ M}_{\odot} \text{ pc}^{-2}$ (relatively uniformly across our sample) at our working resolution of $15''$. Because the THINGS data include observations in the VLA’s most compact (D) configuration, missing flux is not expected to be a large concern. For details see Walter et al. (2008).

The FWHM of the VLA primary beam (field-of-view) is $32'$. In the cases of NGC 5236 (M83) and NGC 5457 (M101), this limits the radii that we can consider to less than $2 \times r_{25}$; in these galaxies the analysis is carried out within $1.7 \times r_{25}$ and $1.5 \times r_{25}$, respectively.

2.3. GALEX UV

To trace recent star formation in the outer disks, we use far UV data from the ‘GALEX Nearby Galaxy Survey’ (NGS, Gil de Paz et al. 2007a). GALEX provides simultaneous imaging in a far UV (FUV, 1350–1750 Å) and a near UV (NUV, 1750–2800 Å) broadband filter

⁸ The National Radio Astronomy Observatory is a facility of the National Science Foundation operated under cooperative agreement by Associated Universities, Inc.

with angular resolutions (FWHM) of $4.0''$ and $5.6''$ respectively, and a field-of-view of 1.25° (for details see Morrissey et al. 2005). We use only the FUV band to trace recent star formation, because it is less sensitive to any old stellar population and suffers less contamination from foreground stars and background galaxies. We use the NUV band to identify foreground stars and to estimate the effects of extinction.

We process the NGS maps slightly. First, we identify foreground stars as regions with an NUV/FUV intensity ratio > 10 and a signal-to-noise ratio > 5 in the NUV maps. We blank these regions after checking the results by eye. In a few cases we adjust the color cut-off to a value higher than 10 to remove particularly bright foreground stars. We also estimate and remove a small background from the FUV maps, which we measure away from the galaxy after discarding emission with intensities more than 3σ above the median value of the image. Finally, we correct the maps for the effects of Galactic extinction, which we estimate from the extinction maps of Schlegel et al. (1998) assuming $A_{\text{FUV}} = 8.24 \times E(B - V)$ (Wyder et al. 2007). In NGC 5194 (M51), we also manually blank the interacting northern companion, M51b.

A typical value for the RMS scatter of the noise in our FUV maps at our working resolution is $\sim 2 \times 10^{-6} \text{ mJy arcsec}^{-2}$ (1σ). The exact value varies significantly from map to map and depends rather sensitively on the method used to derive it. This estimate reflects the median-based scatter (which avoids foreground stars and background galaxies) about the zero level in maps that have already been convolved to $15''$ resolution. Variations in exposure time and map quality lead to a factor of 2–3 scatter in the sensitivity of individual galaxies about the value quoted above.

2.4. Conversion to Physical Units

We convert 21-cm intensity into atomic gas surface density via:

$$\Sigma_{\text{HI}} [\text{M}_{\odot} \text{ pc}^{-2}] = 0.015 I_{21\text{cm}} [\text{K km s}^{-1}] , \quad (1)$$

which yields a hydrogen mass surface density and does not include heavy elements. To convert FUV intensities into SFR surface densities, we adopt the conversion of Salim et al. (2007, their equation 10). For compatibility with previous work (Leroy et al. 2008; Bigiel et al. 2008), we divide their coefficient by an extra factor of 1.59, making the formula appropriate for a Kroupa-type IMF (compare Leroy et al. 2008, Appendix D). Then

$$\Sigma_{\text{SFR}} [\text{M}_{\odot} \text{ yr}^{-1} \text{ kpc}^{-2}] = 0.68 \times 10^{-28} \times I_{\text{FUV}} [\text{ergs s}^{-1} \text{ Hz}^{-1} \text{ kpc}^{-2}] . \quad (2)$$

Salim et al. (2007) derived this calibration for $\sim 50,000$ galaxies by fitting population synthesis models to GALEX UV and SDSS optical multiband photometry. We assume here that the same calibration is applicable to the FUV intensity averaged over large parts of outer galaxy disks. A direct check on this assumption is not straightforward, but Leroy et al. (2008) compared various SFR tracers in the inner parts of many of our target galaxies and found a scatter of $\sim 50\%$, which we will take as our uncertainty in Equation 2. We derive Σ_{SFR}

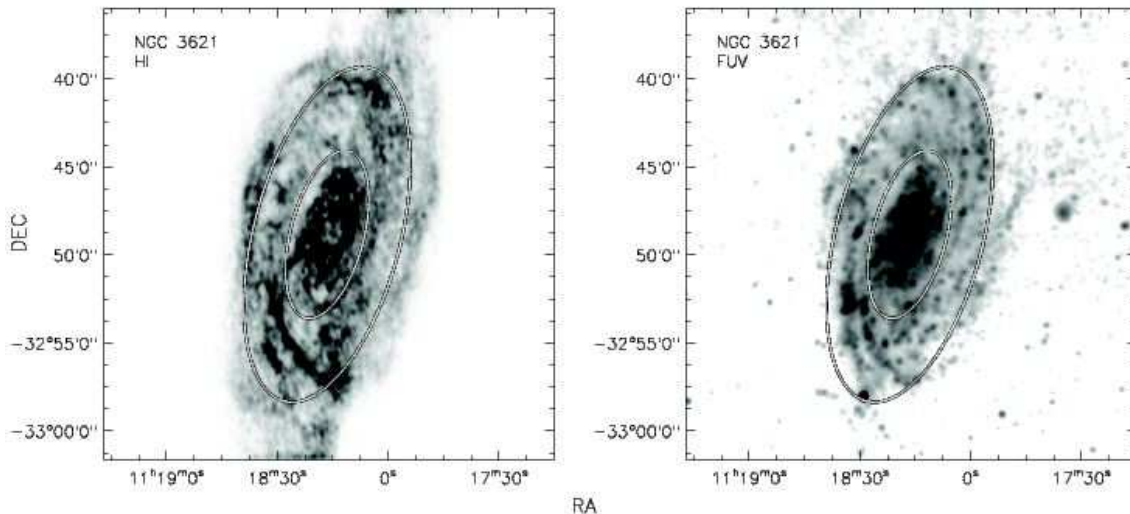


FIG. 1.— THINGS HI (left, linear stretch) and GALEX far UV (right, log stretch) maps for NGC 3621. The ellipses indicate 1 and 2 optical radii (r_{25}) in the plane of the galaxy. In this paper, we compare H I and far UV emission in this regime for 22 nearby galaxies.

from the GALEX FUV maps alone, neglecting the effects of internal extinction. This is both a practical and physical decision. Standard methods to correct for the effects of internal extinction — e.g., combination with IR intensity, use of NUV/FUV color — are largely impossible because of the low signal-to-noise and easy confusion with background sources in this regime. At the same time, we expect the effects of extinction to be small, so that introducing a (noisy) correction factor could easily do more harm than good.

We can estimate a likely upper limit to the bias introduced by neglecting extinction from our H I maps. In the Galaxy, $N(\text{H})/E(B - V) = 5.8 \times 10^{21} \text{ cm}^{-2} \text{ mag}^{-1}$ (Bohlin et al. 1978). This should represent an upper limit to the extinction for a given H I column in outer disks, which have lower metallicities and dust abundances than the Milky Way. If we assume that FUV originates from the midplane (and is thus only affected by half the dust along a line-of-sight) and that $A_{\text{FUV}}/E(B - V) = 8.24$ (Wyder et al. 2007), then $A_{\text{FUV}} = N(\text{HI}) \times 7.1 \times 10^{-22}$ and the FUV intensity corrected for internal extinction is

$$I_{\text{FUV,corr}} = I_{\text{FUV}} \times 10^{N(\text{HI}) \times 2.8 \times 10^{-22}}. \quad (3)$$

For an H I column of $3.0 M_{\odot} \text{ pc}^{-2}$ (i.e., $\sim 3.7 \times 10^{20} \text{ cm}^{-2}$), a typical value between 1 and 2 r_{25} , Equation 3 yields a correction factor of ~ 1.3 . Thus we expect an upper limit to extinction effects to be $\sim 30\%$, and lower at larger radii, where H I surface densities drop significantly below $3.0 M_{\odot} \text{ pc}^{-2}$ and for any region with a dust-to-gas ratio lower than the Galactic average (almost certainly all of our disks).

While we expect that extinction is not a large concern in the outer disks, several plots will display data from within the optical disks (see, e.g., the radial profiles in § 3.1). In this regime, Σ_{SFR} , as defined here, will represent a (significant) underestimate of the true SFR surface density (due to dust extinction). As emphasized above, the conversion between Σ_{SFR} and the (observed) FUV

intensity I_{FUV} is linear and it is thus straightforward to link any of the results or plots in this paper directly to our observables.

3. RESULTS

We employ several approaches to assess the gas-SFR relationship in outer disks. First, we compare radial profiles of H I and FUV between $1 - 2 \times r_{25}$ to test how the overall decline in gas and star formation relate to one another (§ 3.1). Then, we measure the strength of the local correlation between Σ_{SFR} and Σ_{HI} as a function of galactocentric radius (§ 3.2). We subsequently investigate the gas-SFR relationship directly, testing how Σ_{SFR} and the star formation efficiency depend on Σ_{HI} in various regimes (§ 3.3) and carry out a pixel-by-pixel analysis of the outer disk (§ 3.4). We assess the role of large scale gravitational instability as a potential driver for outer disk star formation (§ 3.5) and compare our outer disk data to results for the optical disks of galaxies (§ 3.6) presented by Bigiel et al. (2008).

3.1. Radial Profiles and Exponential Scalelengths

Both H I and FUV emission decline as a function of radius across the outer disks. Because gas is the fuel for star formation, one would expect the SFR to drop in a similar fashion compared to the H I (if all other factors were equal). To test this expectation, we derive radial profiles of each quantity and characterize the decline at large radii using an exponential scale length (i.e., the length over which the emission declines by a factor e).

Figure 2 shows the radial profiles of H I (black) and FUV (gray) together, along with the exponential fits, for our 22 sample galaxies. The profiles are azimuthal averages over beam-wide ($15''$), concentric elliptical annuli constructed using inclination and position angles from Table 1. The error bar on each profile point indicates the RMS uncertainty in the mean in that ring. For easy comparison of profiles in different galaxies, we use common Σ_{HI} and Σ_{SFR} axes. The vertical dotted line indicates the innermost data point included in the fit (which is the profile point closest to r_{25}).

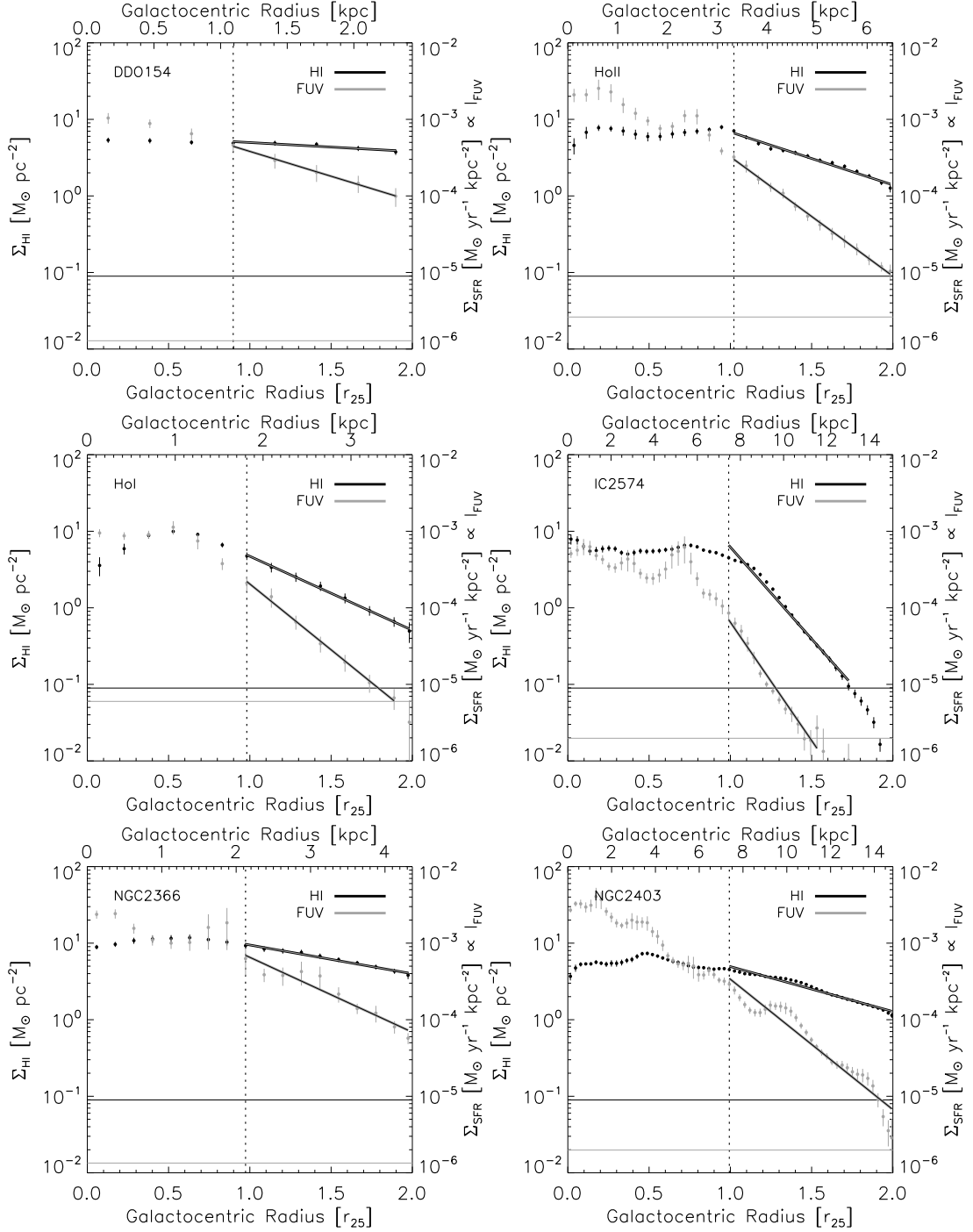


FIG. 2.— Radial profiles of Σ_{SFR} (FUV, gray) and Σ_{HI} (black) for the 22 galaxies in our sample. Error bars on each point show the (1σ) uncertainty in the mean in that ring and horizontal lines (black: HI, gray: FUV) show conservative sensitivity estimates based on the line-of-sight sensitivities in our maps and assuming 20 independent measurements per annulus (note that the FUV sensitivity is sometimes below the lower plot limit). A vertical line indicates the innermost data point included in the fit (approximately at r_{25}). Solid lines show exponential fits to the decline between $1 - 2 \times r_{25}$, only considering points above our sensitivity cuts.

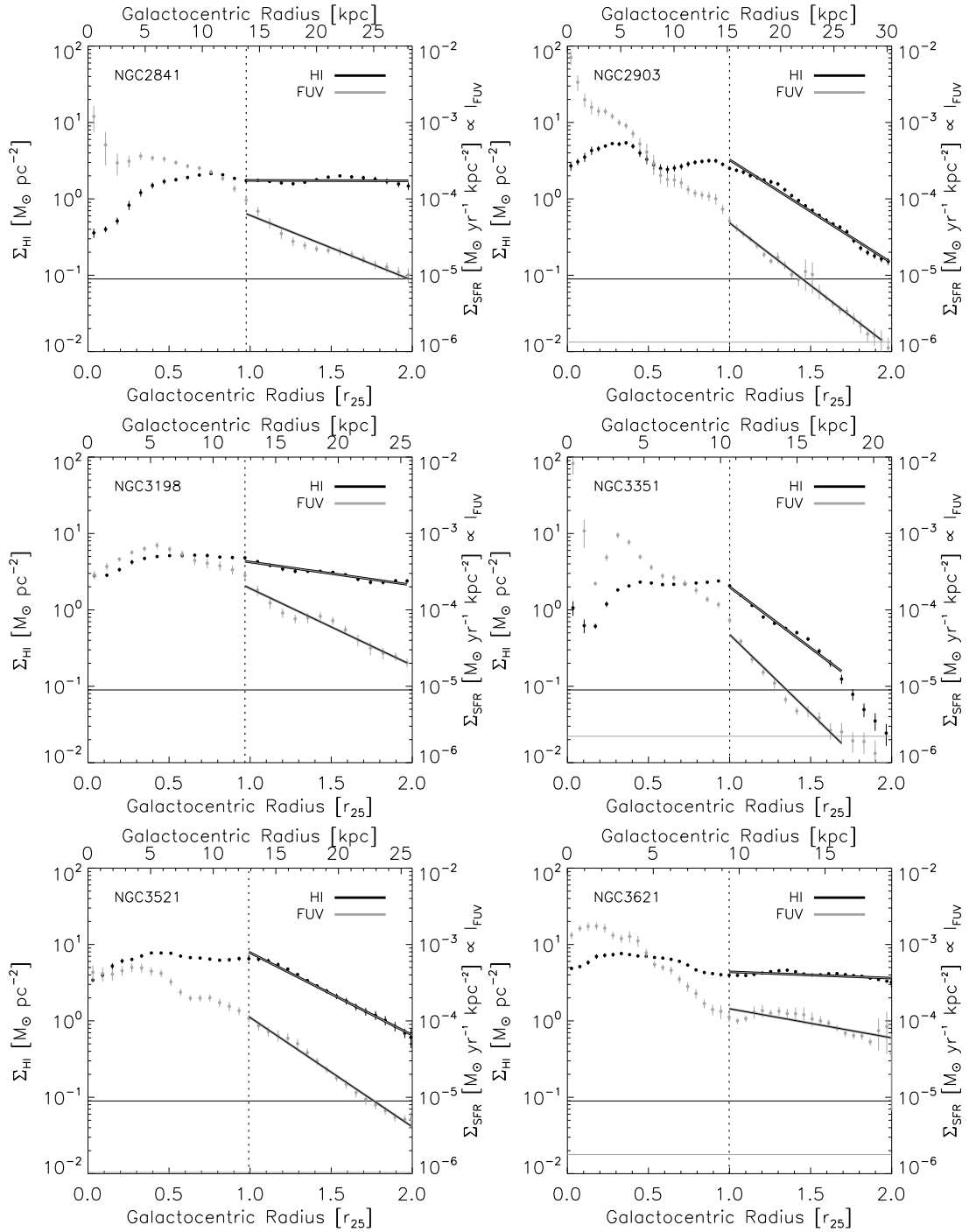


FIG. 2.— continued.

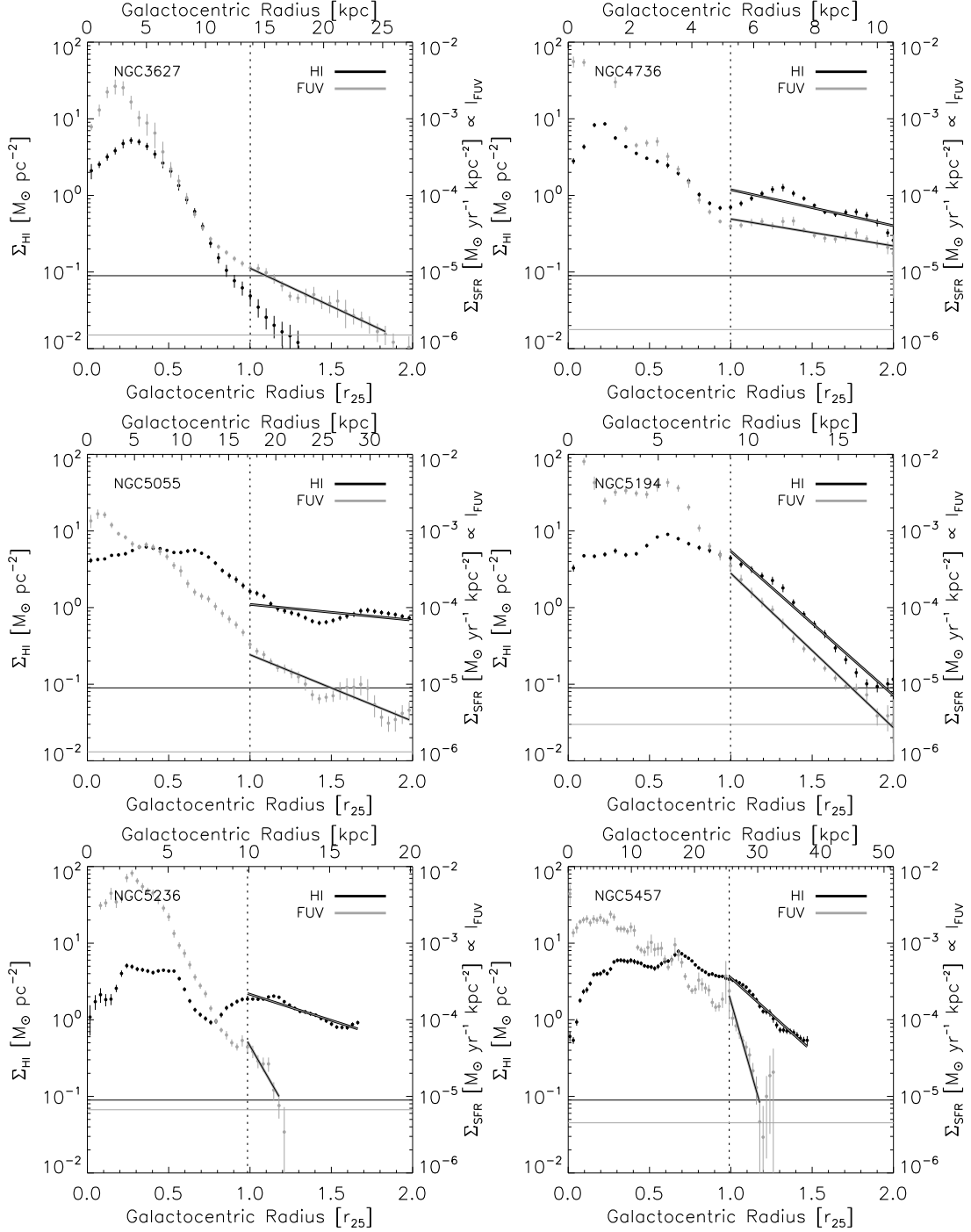


FIG. 2.— continued.

Horizontal lines indicate the sensitivity limits: $0.09 M_{\odot} \text{pc}^{-2}$ for Σ_{HI} (black), a value seldom reached within $2 \times r_{25}$, and the sensitivity (2σ) of each FUV map, converted to units of Σ_{SFR} (gray). To estimate these sensitivity limits we use the H I sensitivity from § 2.2 and the FUV sensitivity from each map and assume (a conservative number of) 20 independent measurements contributing to each annulus to reflect the gain in sensitivity by azimuthal averaging.

Solid lines show our exponential fits to Σ_{SFR} (gray)

and Σ_{HI} (black). We carry out the fits between ~ 1 (the vertical dotted line) and $2 \times r_{25}$ and consider only profile points above our sensitivity cuts. We reiterate that for NGC 5457 and NGC 5236 the field-of-view of our H I maps is too small to probe out to $2 \times r_{25}$. We thus blank their radial profiles outside their respective limiting radius (compare § 2.2). We note that NGC 3627 has too few data points above the H I sensitivity cut to fit the profile beyond r_{25} . We also note that in particular NGC 5236 (M83) is known to have extended FUV fea-

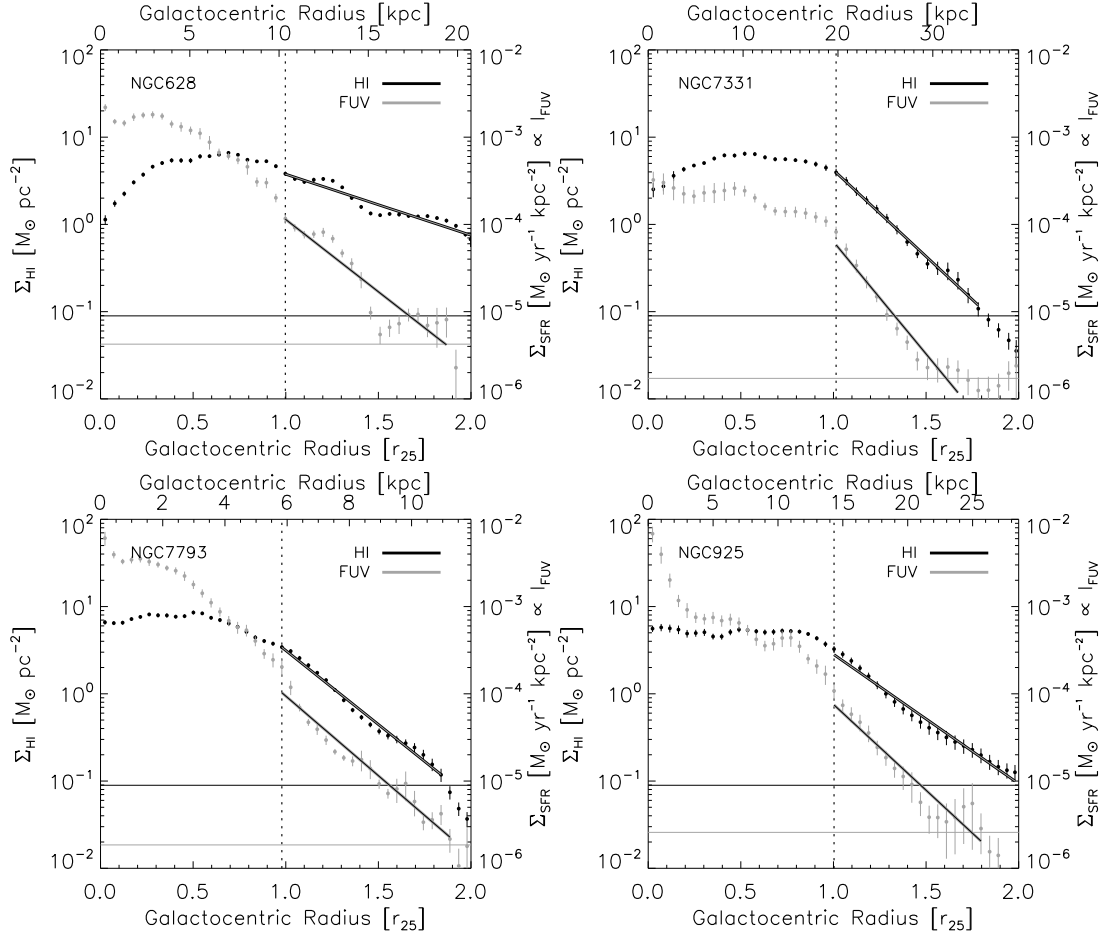


FIG. 2.— continued.

tures in the outer disk (e.g., Thilker et al. 2005). These features have a very low filling fraction for the outer disk annuli and are thus not easily visible in our radial profiles. This galaxy is subject of a separate paper where significantly deeper and more extended data are used to assess the relationship between H I and FUV emission out to many optical radii (Bigiel et al. 2010).

To fit the profiles we use an ordinary least-squares (OLS) approach and estimate the uncertainties in the resulting fit in several ways: by adding noise and re-fitting, bootstrapping (resampling with repeats), varying the radii used to define the fit, and considering only a subset of azimuthal angles (rather than the whole ring).

In fact, azimuthal variations within a galaxy appear to dominate the uncertainty in the fit, which might be expected from the common appearance of streamers, tidal features, and outer arms in both the H I and SFR maps. To separate out this effect, we derive four independent scale lengths for each galaxy, one for each of four sectors with a 90 degree opening angle. The remaining factors (bootstrapping, radius definition, noise) contribute to an uncertainty in the scale lengths for each sector. The typical scatter among the four sector scale lengths is $\sim 0.1 \times r_{25}$, with significantly less scatter in the FUV profiles than the H I (indicating a higher degree of azimuthal symmetry in the FUV emission than in the H I).

Figure 3 shows H I scale length as a function of FUV

scale length. Each galaxy contributes four points, one from each 90°-wide sector, with points for a galaxy sharing the same color and symbol. Black points represent dwarf galaxies, otherwise color is arbitrary. Four galaxies (DDO 154, NGC 2841, NGC 3198, NGC 3621) and 9 individual sectors are omitted from this plot because their H I profiles are too flat to be fit robustly over the range we consider. Their profiles do appear to decline roughly exponentially, but the derived scale length is $> 1 \times r_{25}$, yielding too small a dynamic range for a robust fit. NGC 3627 is also omitted as there are too few data points above the sensitivity limit to fit the H I profile (see above).

Figure 3 demonstrates that in almost every outer disk quadrant we study, the surface density of star formation traced by FUV emission drops more quickly than the surface density of gas (for comparison, the dashed line shows equality). An exception is one sector in NGC 925 (filled purple diamond) which shows a slightly larger FUV scale length (though with large associated uncertainties). Even though generally there is a steady decline in both H I and FUV with radius (Figure 2) and a clear correlation between the scale lengths of the two declines, these declines are not identical. Instead star formation drops with roughly half the scale length of the H I. This is illustrated by the solid line, which shows the mean ratio of FUV scale length and H I scale length

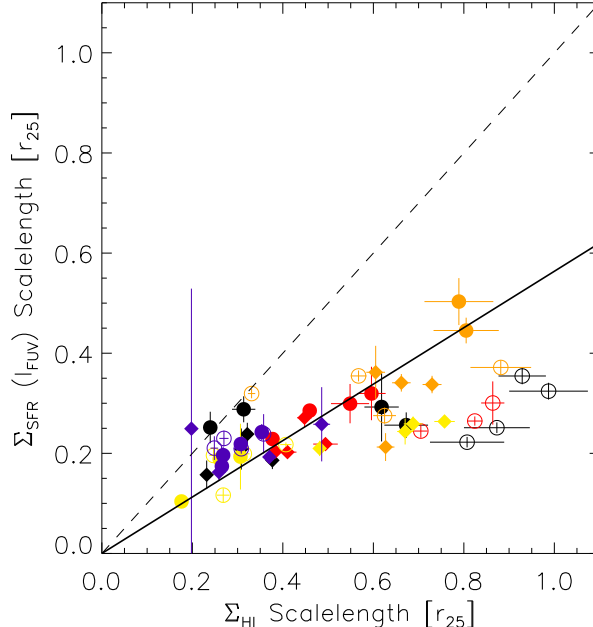


FIG. 3.— Scale lengths for the exponential decline of FUV (y -axis) and HI (x -axis) in outer galaxy disks. Each galaxy contributes four independent measurements from different azimuthal sectors; data points that belong to the same galaxy share the same color and symbol. Black data points represent dwarf galaxies. The dashed line indicates a slope of unity. Virtually all data lie underneath this line, indicating that the FUV profiles generally decline more rapidly than the HI profiles. The solid line, which shows the mean ratio of the two scale lengths, has a slope of ~ 0.5 , i.e., the outer disk HI scale length is twice as large as the FUV scale length on average.

of 0.5 (the 1σ scatter about the mean is ~ 0.2). Therefore, and despite the remarkable extent of star formation revealed by GALEX, it is worth bearing in mind that this widespread UV emission is still relatively centrally concentrated compared to the HI.

3.2. Local Correlation

Comparing radial profiles tells us about the bulk behavior of HI and FUV in outer disks, but does not reveal information about any local relationship. To assess the detailed relationship between FUV and HI, we now turn our attention to how the two quantities correlate on a line-of-sight by line-of-sight basis at a given galactocentric radius. Our approach is to divide each galaxy into 10 equally wide radial bins between the galaxy center and $2 \times r_{25}$ and then compute the Spearman rank correlation coefficient between FUV and HI in each bin. The rank correlation coefficient (Press et al. 1992), r , is a non-parametric measure of the strength of any one-to-one relationship between two quantities. Possible values range from $r = -1$ to 1, with $r = 1$ indicating a perfect correlation — i.e., that the brightest data point in HI is associated with the brightest data point in FUV, the second brightest in HI with the second brightest in FUV, etc. — but giving no information on the functional form. On the other hand $r = 0$ indicates a lack of correlation (expected if the two distributions are independent), while a perfect anti-correlation will yield $r = -1$.

Figure 4 shows r as a function of normalized galactocentric radius for the spiral (left) and the dwarf (right) galaxies separately. Each gray data point represents r measured for one galaxy in one $0.2 \times r_{25}$ -wide radial bin (for better visibility we add a small amount of noise to the x -position to distinguish individual measurements in

the same bin from one another). The vertical error bars show the scatter in r derived from randomly pairing HI and FUV data for that bin; this process destroys any correlation, yielding $r \approx 0$ and the scatter observed repeating the process 100 times gives us an estimate of the uncertainty (this is most rigorously thought of as how confident we are that $r \neq 0$). The black line condenses the gray points into a single trend by giving the median correlation coefficient for all galaxies in each radial bin with error bars indicating the 1σ RMS scatter among galaxies.

For spiral galaxies, r rises from ~ 0.1 near galaxy centers to ~ 0.7 at about r_{25} and then drops again to ~ 0.3 near $2 \times r_{25}$. To assess whether the low values of r at very small and very large radii still represent statistically significant correlations, we extend the procedure that we used to estimate the errors for the individual measurements. We randomly pair HI and FUV data (now for all spirals and dwarfs, respectively), so that $r = 0$ by construction, and bin these data and then derive σ from the scatter in r about the known true value of 0. This exercise leads us to estimate $1\sigma \lesssim 0.04$ for the median profiles in both the spiral and dwarf sample, implying that the median r is significantly different from 0 in the outer parts of spirals but is consistent with 0 within the uncertainties in the inner parts of spirals and the outer parts of dwarf galaxies.

Inside $\sim 0.2 \times r_{25}$, the distributions of HI and FUV are compatible with the hypothesis that $r = 0$, i.e., that the two quantities are unrelated. This regime is not the focus of this study, but the result is easy to understand given that we neglect internal extinction, which is significant in this regime, and molecular gas, which dominates the gas budget in the ISM at these radii.

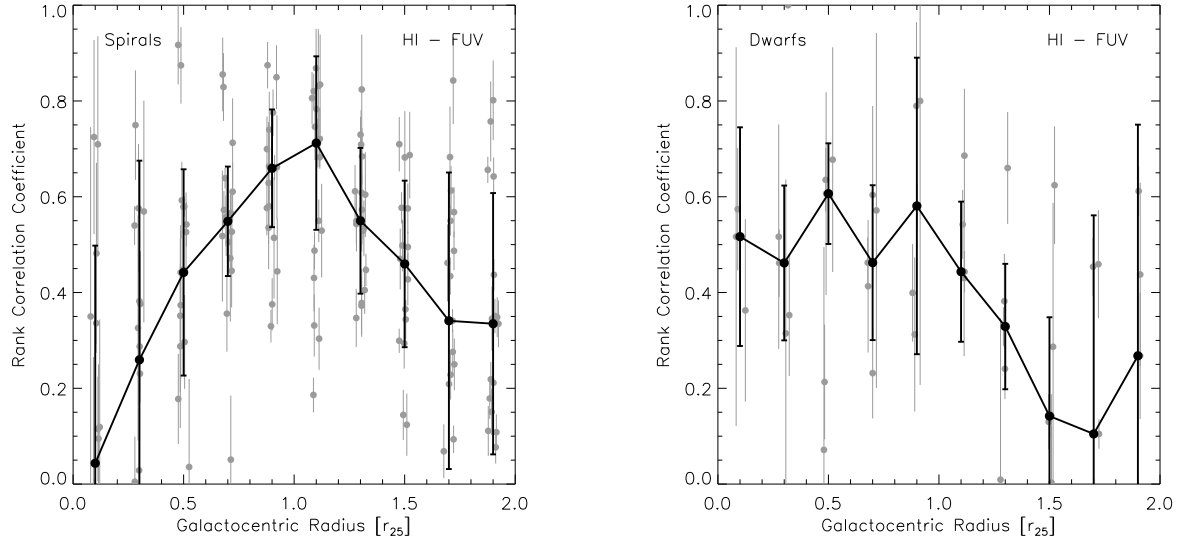


FIG. 4.— Spearman rank correlation coefficient, r , relating HI and FUV as a function of galactocentric radius in the spiral (left) and dwarf (right) galaxies. For each galaxy, we measure r in 10 radial bins spaced evenly between the galaxy center and $2 \times r_{25}$. Each of these measurements, r for one radial bin in one galaxy, appears as a gray point. Vertical error bars show Monte Carlo uncertainty estimates. The black curve in each panel indicates the median r over all galaxies in each radial bin. Black error bars show the 1σ RMS scatter among galaxies in that bin. FUV and HI emission are significantly correlated, with $r \gtrsim 0.5$, around the optical radius in the spirals and throughout the optical disks of the dwarf galaxies. In the inner parts of the spirals extinction and the (unaccounted for) presence of H_2 weaken the correlation. Outside the optical radius, r decreases with increasing radius in both dwarfs and spirals.

The effects of molecular gas and internal extinction should be negligible in outer disks. The decrease in r from its peak near the optical radius towards larger galactocentric radii appears to represent an intrinsic weakening of the correlation between star formation and total gas in this regime.

Maps of both FUV and HI in outer galaxies are often dominated by tidal streamers, arms or other relatively narrow but extended features. One way that the result in Figure 4 might arise even in the face of a one-to-one correlation between star formation and gas is if such features exist but are systematically offset between the HI and FUV maps. To check this possibility, we repeat the analysis in this section with a set of maps convolved to $30''$ resolution. If a small systematic offset were driving the behavior at large radii in Figure 4, we would expect r to increase at lower resolution. We do not find such an effect, suggesting that systematic offsets in otherwise perfectly matched maps do not drive the observed decline in r with radius.

Dwarf galaxies (right panel, Figure 4) do not exhibit the depression in r at small radii seen in spirals, which can be explained because extinction and the contribution of H_2 to the total gas budget are generally small even in the inner disks of dwarf galaxies. It is not clear if the slightly lower r at large radii found in dwarfs compared to spirals is real or a statistical artifact: our sample of dwarfs is small (5) compared to our sample of spirals (17) and the galaxies themselves are smaller, leading to fewer independent line-of-sight measurements per galaxy. The outer disks of dwarf galaxies do show, however, a decline in r with increasing radius similar to that seen in the spirals.

3.3. The Star Formation Efficiency in Outer Disks

We have seen that HI and FUV emission exhibit different radial behaviors (Section 3.1) and that the local

correlation between the two declines from good ($r \approx 0.7$) near r_{25} to poor ($r \approx 0.3$) near $2 \times r_{25}$. The first result means that the rate of star formation *per unit gas* changes systematically across outer galaxy disks while the second implies that quantities other than the local gas reservoir may be important to set this quantity. Here we directly investigate the variation of the rate of star formation per unit gas with HI column and radius in outer galaxy disks. Following convention for extragalactic studies, we refer to the star formation rate per unit gas (here FUV-per-HI) as the star formation efficiency (SFE). This is the inverse of the gas depletion time (τ_{dep}^{-1}), the time required for present day star formation to consume the available gas reservoir; it is sometimes quoted as a true (dimensionless) efficiency by normalizing to 10^8 yr (i.e., quoting the fraction of gas consumed every 10^8 yr). The three formulations are all equivalent within a constant. All SFEs (depletion times) quoted in this paper include a factor of 1.36 to account for heavy elements.

In the remainder of this section, we analyze a data set of matched HI and FUV intensities, each measured over an individual line of sight at $15''$ resolution and together covering the area between 1 and $2 \times r_{25}$ for our whole sample. We extract these data from the maps following the approach used by Bigiel et al. (2008) to study star formation inside the optical disk. Briefly, we measure the intensity from the maps (convolved to $15''$ resolution) at non-overlapping sampling points (i.e., separated by approximately a beam width) and spaced evenly to cover the area between r_{25} and $2 \times r_{25}$ in each galaxy. Each data/sampling point is assigned a weight equal to the inverse of the total number of data points for the galaxy from which it is drawn. We apply these weights when combining data in order to give equal weight to each galaxy; this avoids a few large galaxies dominating all of our plots. Other details are as in Bigiel et al. (2008).

3.3.1. Distribution of H I Columns

Before we examine how the SFE depends on H I column density, it will be useful to see the actual distribution of H I columns in our data. We show this in Figure 5 via normalized Σ_{HI} histograms for the spiral (left panel) and the dwarf (right panel) samples. The dotted histograms show the relative distribution of H I columns across the entire outer disks (between $1-2 \times r_{25}$), where we divided the H I surface density range from $0.4 - 15 M_{\odot} \text{ pc}^{-2}$ into 10 equally wide bins (there are very few data points at higher columns and the lower limit corresponds to the sensitivity of the H I maps). In constructing the histograms, we give equal weight to each galaxy rather than each data point. We test the robustness of the histograms by repeatedly adding noise to the original data and rebinning. Noise and false positives from regions below the sensitivity cut only scatter the results by a few percent.

Unsurprisingly, the dotted histograms in Figure 5 show that low H I surface densities dominate outer galaxy disks. The 50th percentile surface density is $\sim 1.6 M_{\odot} \text{ pc}^{-2}$ for spirals and $\sim 2.3 M_{\odot} \text{ pc}^{-2}$ for dwarf galaxies. The spiral histogram appears approximately exponential, with an e -folding every $\sim 1.6 M_{\odot} \text{ pc}^{-2}$. The dwarf histogram, which is based on fewer data, shows a shallower decline with a suggestion of a flattening at low columns. Broadly, higher column densities are more common in the outer parts of dwarf galaxies than in spirals.

We will also be interested in how the distribution of Σ_{HI} varies with radius. The other histograms in Figure 5 show this. We divide the data into three radial bins ($0.5-1.0 r_{25}$, $1.0-1.5 r_{25}$, and $1.5-2.0 r_{25}$) and then separately plot the same kind of normalized histograms for each bin.

The relationship between dwarfs and spirals does not change dramatically with radius. Spirals (left) show a steeper distribution of Σ_{HI} than dwarfs (right) at all radii, so that dwarfs always have more high-column H I than spirals. Both spirals and dwarfs do show a significant evolution in Σ_{HI} with radius: The fraction of low H I surface densities increases strongly with increasing galactocentric radius and at the lowest radii, Σ_{HI} flattens. The distribution even turns over for dwarfs, so that low H I columns are not the most common values (instead $\Sigma_{\text{HI}} \sim 4 - 6 M_{\odot} \text{ pc}^{-2}$ is the most common value in dwarfs between 0.5 and $1.0 r_{25}$).

3.3.2. SFE vs. H I Column

Figure 6 shows the SFE as a function of Σ_{HI} for data between 1 and $2 \times r_{25}$. We bin the data by Σ_{HI} , assign equal weight to each galaxy and plot the median SFE and Σ_{HI} in each bin. Error bars indicate the 1σ RMS scatter among the data. Very few data contribute to the highest column bins and as a result we cannot robustly estimate the scatter there.

The measurements in Figure 6 appear to all be statistically significant. We check this by repeating the measurement after substituting a pure noise map for the FUV map and by directly propagating the statistical uncertainty in the two maps to derive the uncertainty in the median for each bin. A pure noise measurement would be well off the bottom of the plot and the formal uncertainty in each bin is extremely small (as might be expected from the large number of data).

The figure shows that aside from a slight offset the outer disks of the dwarfs and the spirals exhibit a very similar SFE at a given H I surface density. In both cases, the SFE is a clear function of Σ_{HI} , increasing with rising H I column density. Power law fits to the points in Figure 6 (solid lines) yield indices of 0.7 ± 0.1 for both spirals and dwarfs. Although we saw above that the distribution of Σ_{HI} does differ slightly between the outer disks of spiral and dwarf galaxies, Figure 6 supports the idea that the outer disks of spirals and dwarf galaxies represent similar regimes regarding the regulation and timescales of star formation and that Σ_{HI} may be key to this regulation in this regime.

Studying a subset of our spiral sample, Leroy et al. (2008) and Bigiel et al. (2008) found a constant SFE for the H_2 that dominates the gas reservoir in the inner part of spiral galaxies. The value measured by Bigiel et al. (2008) appears as a dash-dotted horizontal line in Figure 6. Leroy et al. (2008) further found the SFE of the *total* gas to be a well-defined function of galactocentric radius in both spiral and dwarf galaxies; we plot the SFE at r_{25} predicted by their fit for each subsample as dashed lines. Comparing our current data to these lines we see that the SFE in outer disks is an order of magnitude or more below that of the star-forming gas in the inner parts of galaxies, so that it will take well in excess of a Hubble time to consume the gas reservoir *in situ*. The r_{25} predictions from the Leroy et al. (2008) fits coincide with the high end of our measured SFE, suggesting that the steady decline they find may continue past r_{25} .

3.3.3. Dependence on Radius

Leroy et al. (2008) and Bigiel et al. (2008) found that galactocentric radius was actually a much better predictor of SFE than Σ_{gas} in the inner parts of galaxies, likely because it tracks key environmental quantities like the stellar potential well and metallicity. To assess whether a similar radial gradient for the SFE holds in outer disks, we separate our data into three radial bins — $0.5-1 \times r_{25}$, $1-1.5 \times r_{25}$ and $1.5-2 \times r_{25}$ — and repeat the above analysis (§ 3.3.2) for each bin.

Figure 7 shows the SFE as a function of Σ_{HI} for each radial regime with dwarfs and spirals plotted separately. All plot parameters are identical to Figure 6. Again we plot no error bars if only a few galaxies contribute to a bin. We also plot arrows instead of error bars where the scatter exceeds the lower plot boundary. Reading Figure 7, it is important to bear in mind that the SFE we plot between $0.5 - 1.0 r_{25}$ in spirals is biased (in opposite directions) by our failure to account for internal extinction or H_2 (in these galaxies the ISM appears to be roughly equal parts H I and H_2 at $\sim 0.5 r_{25}$, Leroy et al. 2008); the points in Figure 7 are rigorously FUV-per-H I rather than SFE.

In order to understand the upturn at low H I columns, we traced the data for the lowest H I-column bins back to the original images and found that they mostly arise from local H I depressions (i.e., ‘H I holes’) in regions with diffuse, locally smooth FUV emission. The FUV intensities involved are very low and inside a galaxy disk — the effect appears most pronounced for the inner radius bin in Figure 7, i.e. within r_{25} — interpreting these intensities can be complicated; one might expect some level of FUV emission from any galaxy due to an intermedi-

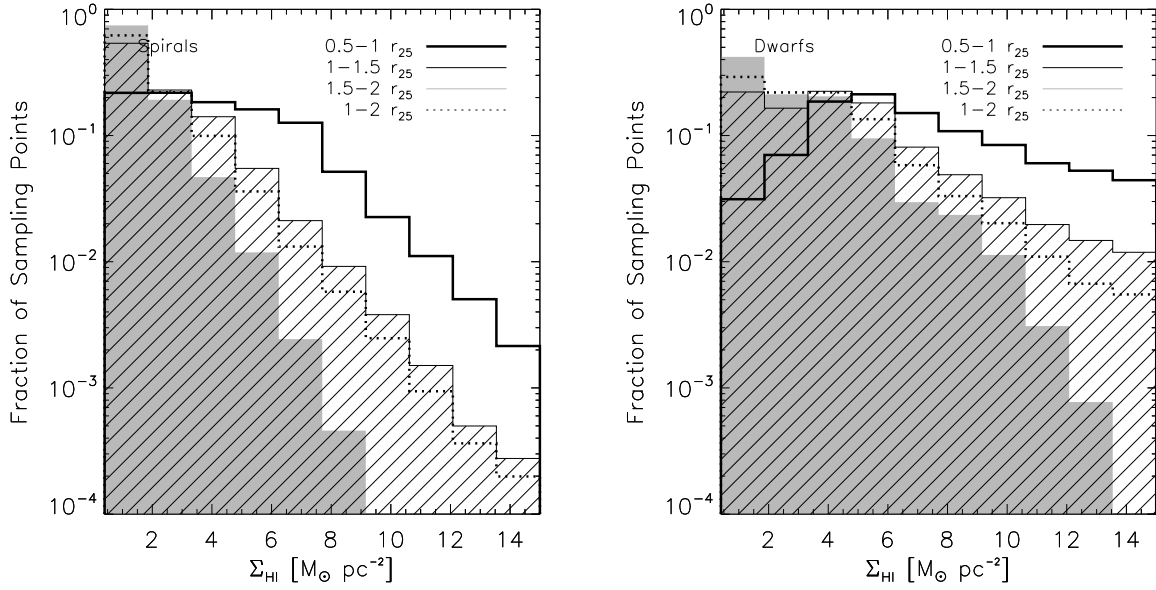


FIG. 5.— The 4 histograms in each panel (left: spirals; right: dwarfs) show the normalized HI histograms between 1 and $2 \times r_{25}$ (black dotted line) and for 3 other radial regimes: $0.5 - 1 \times r_{25}$ (thick black line), $1 - 1.5 \times r_{25}$ (black hashed) and $1.5 - 2 \times r_{25}$ (filled gray). Every galaxy is assigned equal weight. In particular for the spirals, there is an approximately exponential decline in frequency with increasing Σ_{HI} , with dwarfs showing a much shallower decline and more high-column data. Each dwarf histogram is systematically shallower than the respective one for the spirals and with increasing radius, the fraction of sampling points with low HI columns increases strongly at the expense of those with high HI columns.

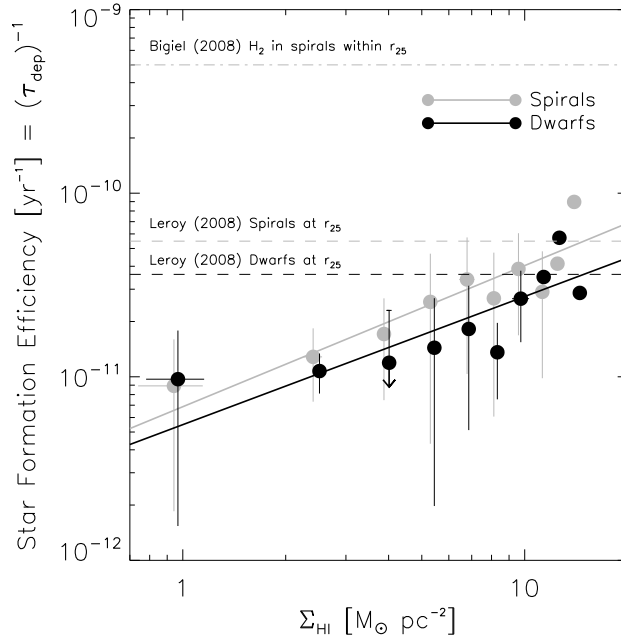


FIG. 6.— SFE (i.e., SFR/gas or FUV/HI) binned by Σ_{HI} for both samples (spirals: gray; dwarfs: black). Individual filled circles represent the median SFE and Σ_{HI} , error bars the 1σ RMS scatter in each bin (error bars are omitted on the highest two bins because only little data contribute). Every galaxy is assigned equal weight. The solid lines indicate power law fits to the two distributions (both cases have slope ~ 0.7). Horizontal lines illustrate various comparison measurements: the SFE of molecular gas within the optical disks of spirals and of total (atomic plus molecular) gas at r_{25} in dwarfs and spirals. The SFE is lower in outer disks than within the optical disk and rises with increasing HI column, showing a similar behavior in dwarfs and spirals.

ate age population, dust-scattered FUV light, or evolved stars. Therefore, while Figure 7 shows the real trend in our data we emphasize the systematic uncertainty in the lowest bins, particularly at low radii.

At higher $\Sigma_{\text{HI}} (\gtrsim 5 M_{\odot} \text{ pc}^{-2})$ all radial regimes in both subsamples exhibit a positive correlation between SFE and Σ_{HI} similar to what we saw in Figure 6 for the entire outer disks. The other general trend evident for spirals is a decrease in SFE with increasing radius at fixed Σ_{HI} . For the dwarf sample the radial behavior is much less clear. A decline in FUV per H I with increasing radius is clearly present at low Σ_{HI} , but whether this represents a real decline in SFE depends on one’s interpretation of the low FUV intensities.

3.4. Local Relations in Outer Disks

3.4.1. Star Formation and H I

We have so far binned and averaged our data to compare H I and FUV in a number of ways. It is also interesting to examine how individual data are distributed in $\Sigma_{\text{SFR}}\text{-}\Sigma_{\text{gas}}$ (FUV-H I) parameter space. Here we plot FUV as a function of H I directly for the data assembled in Section 3.3. This allows ready comparison to work on the inner parts of galaxies by Bigiel et al. (2008) and numerous literature measurements aimed at constraining the star formation law (e.g., Kennicutt 1998).

We have many thousands of data points, making a direct scatter plot impractical. Therefore, we convert the data into two-dimensional density distributions, again giving each galaxy equal weight. Figure 8 shows the resulting data density using contours to indicate the area containing the densest 25% (magenta), 50% (red), 75% (orange), and 90% (green) of the data. The data distributions in Figure 8 and the corresponding distributions inside r_{25} are available as supplemental online material.

Many of the conclusions from Sections §3.3.1 and §3.3.2 are again evident in Figure 8. Depletion times are large (lines of constant H I depletion time appear as dotted diagonal lines in Figure 8) and change systematically but relatively weakly with changing Σ_{HI} . Dwarf galaxies exhibit somewhat higher Σ_{HI} than spirals, leading to a lack of low-column points in the right panel of Figure 8. At a given H I column density, the FUV one finds in spirals and dwarfs is quite similar. This last conclusion can be clearly seen from the right panel of Figure 8, where the orange contour from the left panel appears as a thick black contour that closely matches the distribution observed in dwarfs.

Sensitivity is a significant concern in this plot. The horizontal line shows a typical 3σ sensitivity for our FUV maps. A large fraction of our measurements lies below this line. This is problematic for a log-log plot, where negatives are not reflected. To robustly follow the general trend down to low Σ_{SFR} , we overplot median values for Σ_{SFR} in 5 equally spaced Σ_{HI} bins as black circles. All data, including negatives, contribute to the median, making it much more sensitive than each individual point. Error bars on these points give our best estimate for the intrinsic (log) scatter in Σ_{SFR} in each H I bin. We derive this estimate by comparing the observed data in each bin to a series of mock data distributions. These are constructed to have the observed median and appropriate Gaussian noise (measured from the FUV maps)

with varying degrees of lognormal scatter (from 0.0 to 2.0 dex). We compare each mock distribution to the observed data using a two-sided Kolmogorov-Smirnov (KS) test (Press et al. 1992). The scatter that generates the distribution most similar to the observed data is our best estimate for the true intrinsic scatter.

For H I columns $\gtrsim 3 M_{\odot} \text{ pc}^{-2}$, the scatter for both spirals and dwarfs is a few tenths of a dex (1σ), so that knowing the H I column (and that one was in an outer galaxy disk) could serve as an estimate for Σ_{SFR} with an accuracy of a factor of 2-3. While this continues to be true at low columns in dwarf galaxies, the scatter increases significantly below $\Sigma_{\text{HI}} \sim 3 M_{\odot} \text{ pc}^{-2}$ for spirals (although the median Σ_{SFR} for spiral and dwarf galaxies is still roughly the same at these columns). If the observation is real and not an artifact of poor statistics in the dwarf sample it may reflect a wider range of environments in the outer disks of spiral galaxies.

One feature that particularly stands out in Figure 8, but was not evident earlier, is an apparent maximum to the SFE in outer galaxy disks. Almost all data have H I depletion times longer than $\sim 10^{10}$ yr (this line is a rough upper envelope to the green contour in both panels). This implies that at their present SFR, even the most efficient outer disks in our sample will not consume their available gas in less than 10 Gyr (roughly a Hubble time) at their present SFR.

3.4.2. SFE, Radius, and H I

In Figure 9 we use the data to plot the SFE (τ_{Dep}^{-1}) as a function of radius. The corresponding plot showing SFE as a function of H I for individual lines of sight appears as Figure 10. In both plots contour levels and other details are identical to Figure 8. Black filled circles and error bars show the median SFE and best-estimate intrinsic scatter (using the same approach as above) in evenly spaced bins.

Again several earlier conclusions are more clearly visible in Figures 9 and 10: the SFE (τ_{Dep}) does appear to vary systematically with both radius and H I column, but this variation is quite weak compared to the intrinsic scatter in the data (especially for the radial variations in spirals). The difference between the dwarf and spiral samples seems to be largely the distribution of H I columns: at a given column or radius the SFE appears largely similar in the two samples and the range of SFEs found for the two samples is similar ($\tau_{\text{Dep}} \sim 10^{10} - 10^{12}$ yr), with 10^{10} yr a rough lower limit to τ_{Dep} .

These line-of-sight measurements also allow us to look for a star-formation threshold, a set of local conditions below which star formation is suppressed and above which it sets in. In a plot like in Figures 8 or 10, a true threshold as a function of the ordinate should correspond to a rapid decline in the SFE as one crosses the threshold. Neither Figure 8 nor Figure 10 show clear evidence for such a behavior; the SFE varies systematically but does not drop precipitously at any particular H I column density or radius. This does not necessarily rule out a local threshold, but if one exists then the timescales and spatial scales involved must be long enough and small enough to yield a smooth trend of FUV/H I as a function of H I column and radius (albeit one with large scatter).

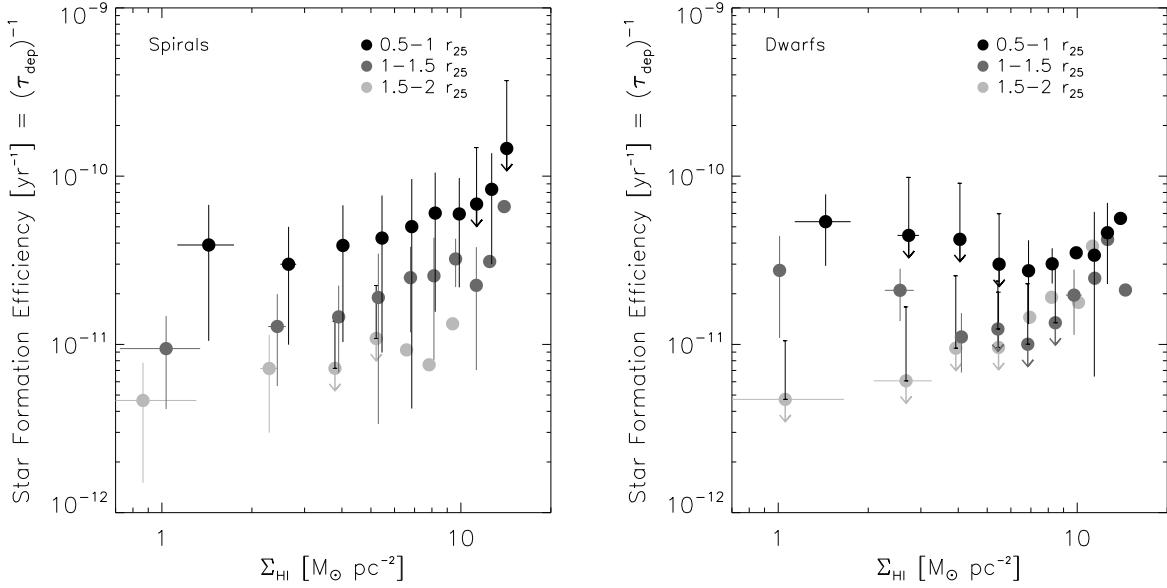


FIG. 7.— SFE as a function of Σ_{HI} for spiral (left) and dwarf (right) galaxies. Methodology as Figure 6 except that the data have now been divided into 3 radial bins with results for each bin plotted separately (black filled circles show radii $0.5 - 1 \times r_{25}$, dark gray circles from $1 - 1.5 \times r_{25}$ and light gray circles from $1.5 - 2 \times r_{25}$). We also plot arrows instead of error bars where the scatter exceeds the lower plot boundary. Generally, the SFE increases with Σ_{HI} and for a given Σ_{HI} , the SFE decreases with increasing galactocentric radius.

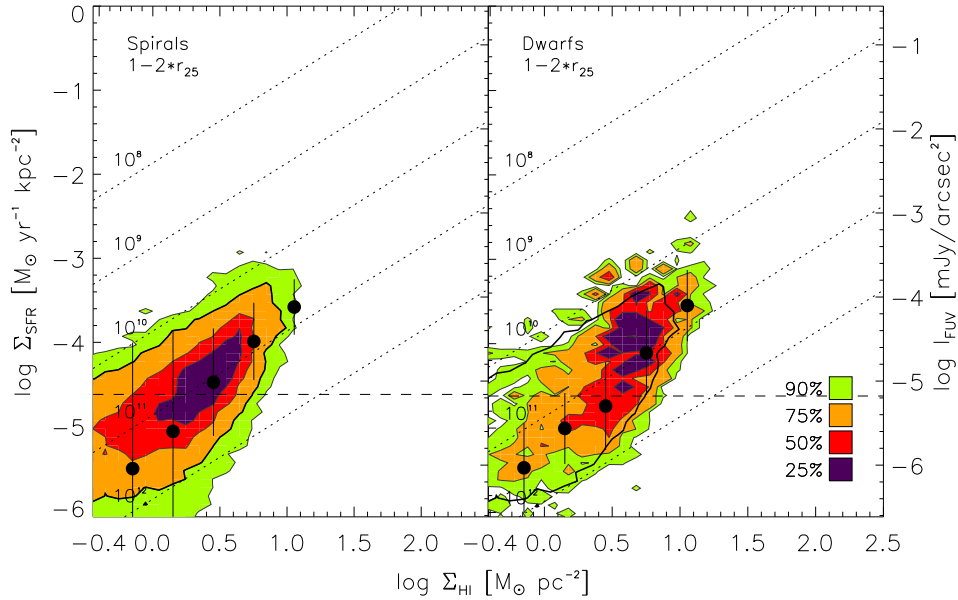


FIG. 8.— Pixel-by-pixel distribution of FUV (right axis; left axis after conversion to Σ_{SFR} , Equation 2) as a function of HI in the outer disks ($1 - 2 \times r_{25}$) of spiral (left) and dwarf (right) galaxies. Contours show the density of data after combining all galaxies in each sample with equal weight given to each galaxy. Magenta, red, orange, and green areas show the densest 25%, 50%, 75% and 90% of the data, respectively. Dotted lines indicate constant HI depletion times of 10^8 to 10^{12} yr (taking into account heavy elements). A horizontal dashed line indicates the typical 3σ sensitivity of an individual FUV measurement. Black filled circles show our best estimate for the true relation between FUV and HI after accounting for finite sensitivity: they represent the median FUV after binning the data by Σ_{HI} and error bars are the lognormal scatter that yields the best match to the data after accounting for noise (see text). To allow easy comparison, we overplot the orange (75%) contour for the spirals as a thick black contour in the dwarf (right) plot.

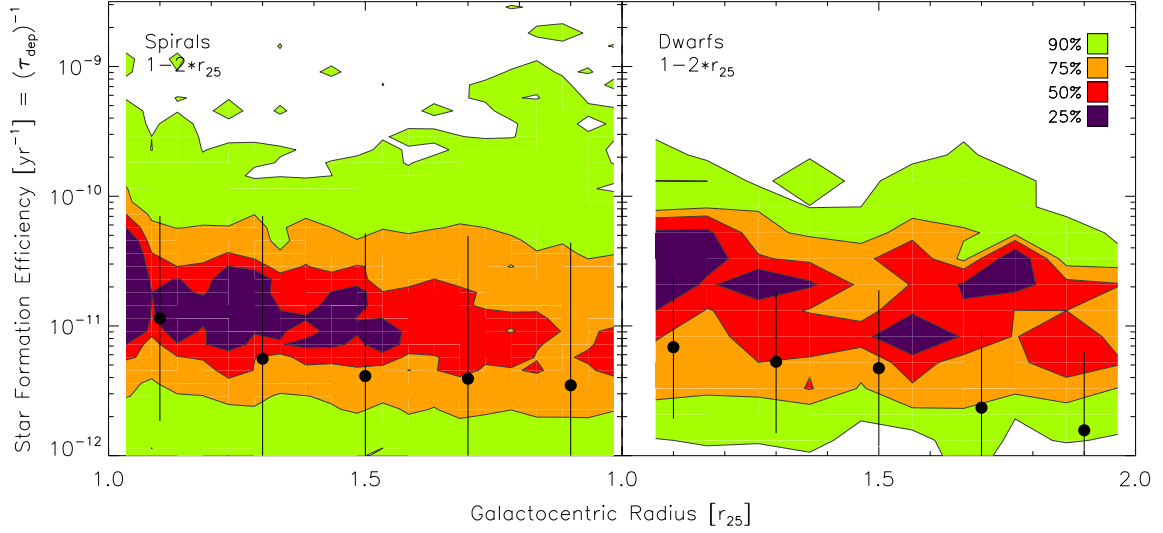


FIG. 9.— FUV-to-HI ratio (SFE or τ_{Dep}^{-1} , y -axis) as a function of galactocentric radius in the outer disks of the spiral (left) and dwarf (right) galaxies. Contour levels, medians (black circles) and estimated intrinsic scatter (black error bars) are derived as for Figure 8 (also compare text). As for the SFR-HI plots in Figure 8, both distributions are found to look almost identical, supporting the previous finding that the outer disk data from both galaxy samples lack clear distinguishing characteristics regarding their star forming properties. The SFE for both samples shows only mild variations across the outer disks.

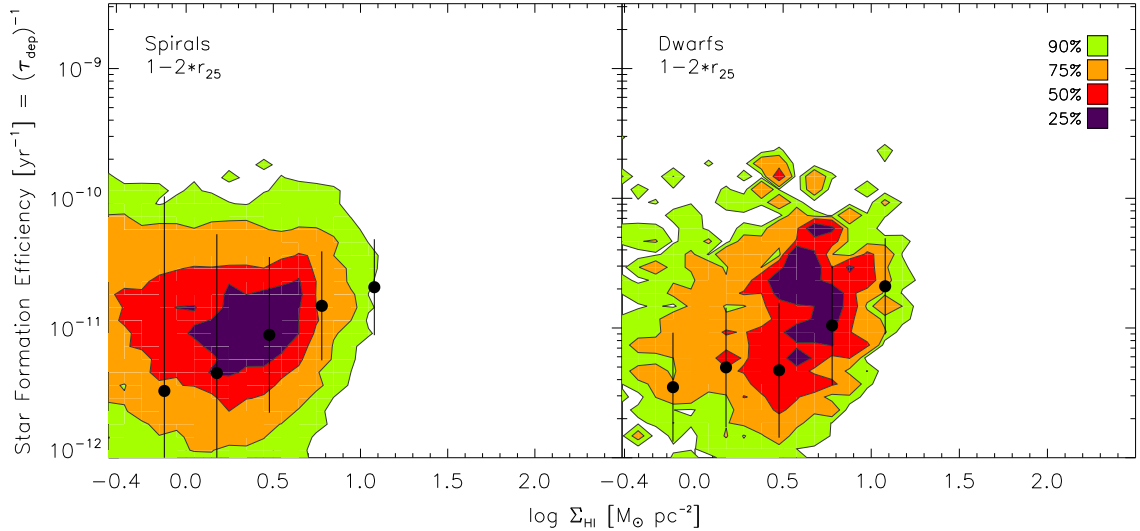


FIG. 10.— The SFE (τ_{Dep}^{-1}) as a function of HI surface density Σ_{HI} for outer galaxy disks ($1 - 2 \times r_{25}$) in spiral (left) and dwarf (right) galaxies. Contour levels, the methodology used to derive the median SFEs (black circles) and associated scatter, and other plot parameters are identical to the previous figures. We do not find an obvious discontinuity in the the SFE as a function of Σ_{HI} (as one might expect for a star formation threshold). Instead the SFE changes relatively smoothly as a function of Σ_{HI} with significant scatter.

3.5. Toomre's Q in Outer Disks

Toomre's Q parameter (Toomre 1964), which measures the stability of a thin axisymmetric disk (or ring, if the galactocentric radius is kept as a free parameter), has been closely linked to the decline of star formation in outer disks (e.g., Martin & Kennicutt 2001). Here we compare Q to the rate of star formation per unit gas in outer galaxies to see if a universal behavior emerges. We calculate Q via

$$Q_{gas} = \frac{\sigma_{gas}\kappa}{\pi G \Sigma_{gas}}, \quad (4)$$

with values < 1 indicating instability (i.e., gas can collapse and form stars) and values > 1 indicating stability (i.e., no star formation). Here σ_{gas} denotes the velocity dispersion of the gas, G is the gravitational constant and κ is the epicyclic frequency. In the outer disks that we study, a flat rotation curve is usually a good approximation (see de Blok et al. 2008) and we can calculate κ from $\kappa = 1.41v_{flat}/r_{gal}$, where v_{flat} is the rotation velocity at large radii. We adopt v_{flat} from Leroy et al. (2008) where available and derive it in a similar manner for galaxies that they did not study. We take $\sigma_{gas} \approx 11$ km/s everywhere, which is a reasonable approximation for the H I velocity dispersion (to within a few km/s) over outer galaxy disks (see Tamburro et al. 2009). Equation 4 assumes the mass budget to be dominated by gas (ignoring the stellar contribution considered by, e.g., Jog & Solomon 1984; Rafikov 2001; Yang et al. 2007); we consider this a reasonable approximation outside r_{25} .

Figure 11 shows the FUV-to-H I ratio as a function of Q . Low values of Q indicate gas that is more unstable to collapse and might thus be expected to correspond to regions of more active star formation per unit gas (e.g., Li et al. 2005; Yang et al. 2007). Such a trend is not obvious from Figure 11, which shows that on the scales we study most gas appears quite stable with little or no local correlation between Q and the FUV-to-H I ratio.

Despite the lack of a strong local trend, there is an overall correspondence: the depletion times that we derive are much larger than those found inside r_{25} , while the typical values of Q in outer disks ($Q_{median} \approx 30$) are, on the whole, much larger than those found inside r_{25} . Inside r_{25} , Leroy et al. (2008) found $Q_{median} \approx 4$ for the same methodology that we use here and $Q_{median} \approx 2$ considering a disk of gas and stars (also see Boissier et al. 2003; Yang et al. 2007). Figure 11 does not offer clear evidence for Q as a 'silver bullet' for star formation thresholds, but outer H I disks are clearly more Toomre stable than gas inside r_{25} (for a discussion of the interplay between H I phases, the gas velocity dispersion, and Q see Schaye 2004; de Blok & Walter 2006).

There are several subtleties to calculating Q : corrections are sometimes applied for disk thickness (stabilizing) and the influence of stars (destabilizing) and the appropriate H I velocity dispersion is a matter of some dispute. We use the median velocity dispersion measured at r_{25} , but using a lower dispersion more appropriate to a cold phase (e.g., $\sigma_{gas} = 6$ km/s instead of 11 km/s) would not change our basic conclusions, as Q would only decrease by a factor of $\sim 2 - 4$ (even before accounting for the fraction of gas in the cold phase, which must be

relatively low given the observed dispersions).

We do also note that there is a significant contribution of dark matter to the local mass volume density in the outer disks. Assuming a flat rotation curve, the local dark matter volume density ρ_{dm} at $1.5r_{25}$ is of the same order as the local H I density, i.e., $\rho_{dm} \approx \rho_{HI}$. Deriving the effect of the dark matter on the disk stability is non-trivial, but even if it were concentrated into a thin disk along with the H I it would not be enough mass to induce formal instability.

3.6. Comparison to Optical Disk Measurements

We have looked at the relation between H I and FUV in outer disks in some detail. What remains now is to try to link these results to the inner parts of galaxies. We do so in the following by comparing our results to those of Leroy et al. (2008) and Bigiel et al. (2008), who studied an overlapping sample of spirals and dwarfs using many of the techniques used here. It is absolutely essential to note that as we do so, we abandon the clean mapping between physical quantities and observables maintained throughout the first part of this paper: Σ_{gas} in Leroy et al. (2008) and Bigiel et al. (2008) includes the contribution of H_2 estimated from HERACLES CO maps (Leroy et al. 2009) and Σ_{SFR} represents a combination of FUV and IR (24 μ m) emission, with the IR usually the dominant term (see those two studies for details). With this caution firmly in place, we now compare the scale length of star formation, the local relation between Σ_{SFR} and Σ_{gas} , and the SFE as a function of radius across the two regimes.

Radial profiles of Σ_{SFR} appear to follow a steady decline with approximately constant scale length from inner to outer disks. We show this in Figure 12, where we plot scale lengths fit by Leroy et al. (2008) to combined UV and IR profiles against our outer disk measurements. There is significant scatter in the plot, but with two notable exceptions the data appear to scatter around equality with $\pm 0.1 r_{25}$ (typically $\sim 50\%$) scatter. The two exceptions are the dwarf irregulars IC 2574 and Ho I, which both show a sharp downturn in their H I and FUV profiles starting just inside r_{25} (see Figure 2).

By contrast, just glancing at Figure 2 makes it clear that the H I does noticeably change its behavior between the inner and outer disk. Our H I profiles are usually fairly flat inside the optical disk (sometimes with central depressions), while almost all of the profiles show a radial decline outside r_{25} . We have already seen that this decline is still shallow compared to the decline in Σ_{SFR} . Leroy et al. (2008) found that the CO and SFR scale lengths were comparable inside r_{25} , so we expect that the decline in H I is also shallower than the decline in CO in the inner disk. This suggests that the total gas (H I + H_2) distribution may follow a broken exponential rather than a single profile.

In Figure 13 we compare individual line-of-sight measurements between the optical and outer disks. Plot parameters largely match Figure 8, though now the outer disk data appear as *unfilled* contours (the median and estimated scatter are still black points with error bars). *Filled* contours show data from within the optical disk (Bigiel et al. 2008, their Figures 8 and 12 with slight changes to methodology: we assign equal weight to each galaxy, use a larger bin width, and define the contours

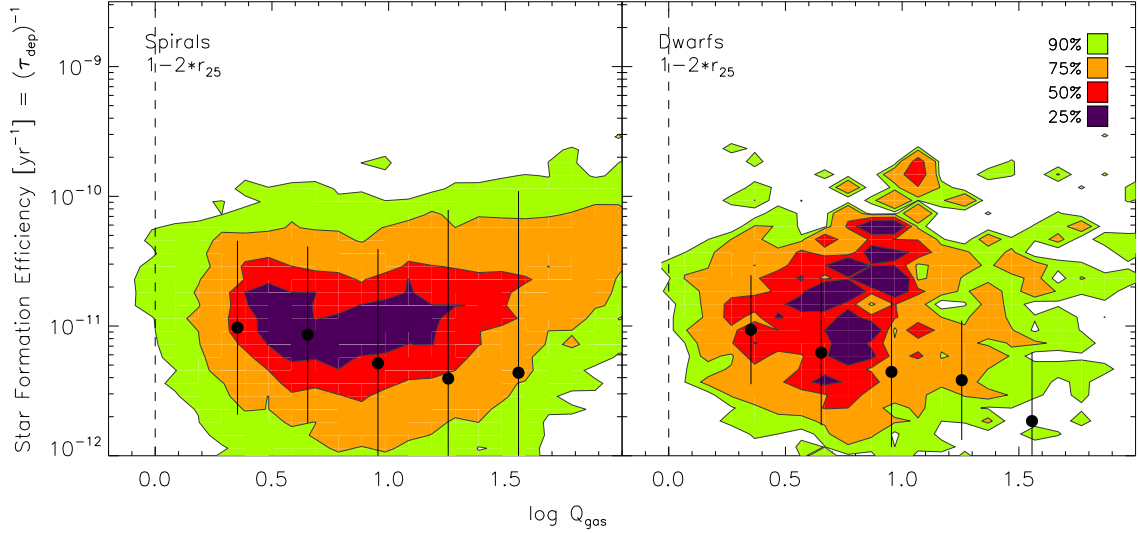


FIG. 11.— FUV-to-HI ratio (SFE, y -axis) as a function of (\log_{10} of) Toomre’s Q parameter (x -axis) in the outer disks of spiral (left) and dwarf (right) galaxies. Details of the plot are as in the previous figures. Q is calculated under the assumption of a flat rotation curve and $\sigma_{\text{HI}} = 11 \text{ km s}^{-1}$ (Tamburro et al. 2009). Almost all of the data are formally stable ($Q > 1$, right of the dashed line). There is no clear trend in the FUV-to-H I ratio (SFE) as a function of Q at $\sim 750 \text{ pc}$ scales, as one might expect if Q was the main criterion for a step-function type star formation threshold.

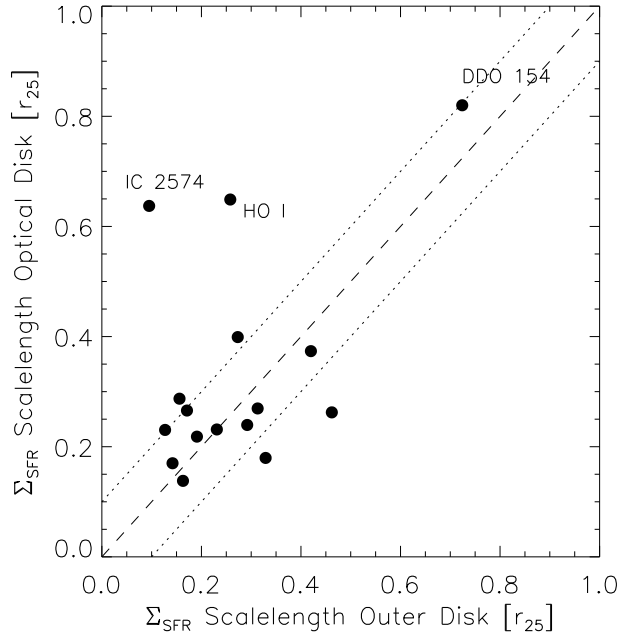


FIG. 12.— Scale lengths of Σ_{SFR} (FUV + IR) measured within the optical disk by Leroy et al. (2008) as a function of our outer disk Σ_{SFR} (FUV) scalelengths for the overlap in samples. The dashed line indicates equality and the dotted lines show $\pm 0.1 r_{25}$. The two quantities agree reasonably well, with only the dwarf galaxies IC 2574 and Ho I showing a sharp truncation in Σ_{HI} as well as in Σ_{SFR} .

via the fraction of data enclosed rather than absolute counts). Tables containing the distribution and sampling data used to construct Figure 13 (optical and outer disk data for the spiral and the dwarf sample) are available as electronic supplemental material.

The outer disks in Figure 13 largely extend the distribution found within the optical radius to lower SFR and gas surface densities. There may be a small discontinuity between the two distributions along the y -axis due to the

inclusion of an IR-based extinction correction inside the optical radius. What is striking is that the outer disk data lie overwhelmingly in a different part of parameter space from data inside the optical disk. In both samples, we see a smooth trend extend to very long depletion times and low gas columns that are almost totally absent inside the optical disks. Also in contrast to the optical disks, a clear trend relating H I and SFR emerges in both subsamples. Inside r_{25} , particularly within $0.5 \times r_{25}$, the

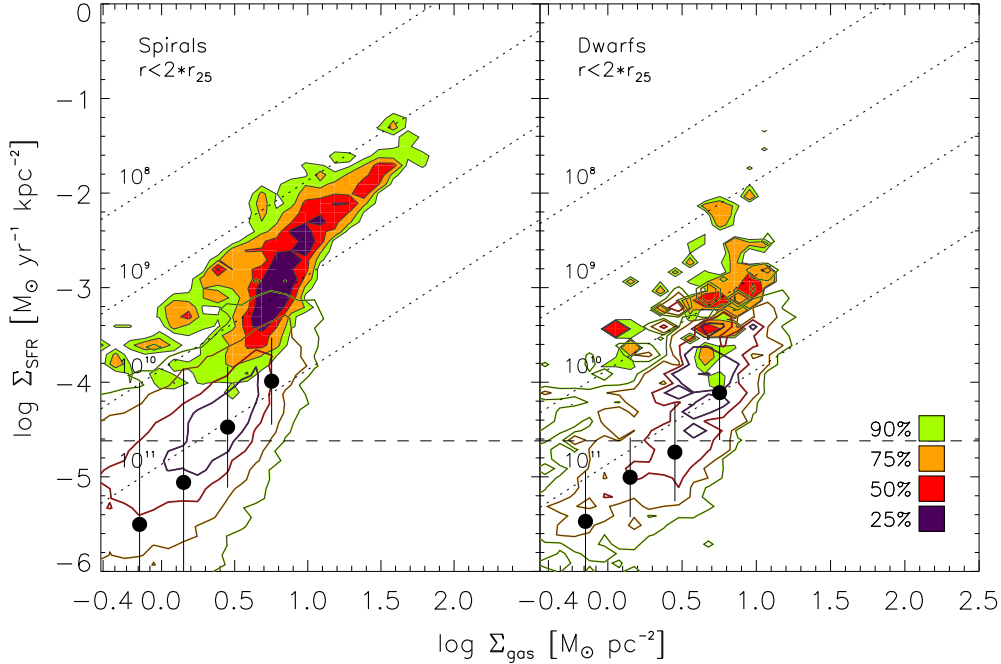


FIG. 13.— Star formation and gas from inner to outer disks (left: spirals, right: dwarf galaxies). Filled contours show the pixel-by-pixel distribution of Σ_{SFR} as a function of Σ_{gas} inside r_{25} (filled contours) for a subset of our sample (Bigiel et al. 2008). Empty contours show outer disk data (see Figure 8) with black filled circles indicating median and scatter. Plot parameters are as in Figure 8. In spirals, the steep relation between Σ_{SFR} and Σ_{gas} seen inside r_{25} becomes more shallow at large radii, leading to relatively modest variations in the median SFE (depletion time) across the outer disks (though the scatter is large). For both spiral and dwarf galaxies, data from inside r_{25} appear to more or less continuously extend into the outer disk. Note that the slight offset in Σ_{SFR} between the outer and inner disk data is due to different methodology in deriving SFRs in the two regimes (see text for details). These data are also available as supplemental online material.

relationship between H I and Σ_{SFR} is weak or nonexistent; instead H_2 is clearly correlated with Σ_{SFR} (Bigiel et al. 2008).

There appears to be a ‘forbidden region’ in Figure 13 at relatively high Σ_{HI} ($\sim 3\text{--}10 M_{\odot} \text{pc}^{-2}$ or $\log(\Sigma_{\text{HI}})$ between ~ 0.5 and 1) and low Σ_{SFR} . This lack of high-H I low-FUV gas combines with the upper envelope of $\tau_{\text{Dep}} \sim 10^{10}$ yr in the outer disks and the turn towards a fixed τ_{Dep} in the H_2 dominated (inner) parts of galaxies to create a combined distribution with an ‘S-like’ shape (though note that there is some gas at low columns with $\tau_{\text{Dep}} \lesssim 10^{10}$ yr inside the optical disks of spirals). We will interpret this combined distribution in Section 4.

The dwarf distributions lack the upper turn to the right in the ‘S-shape:’ we do not observe a significant amount of data at high Σ_{gas} , at least partially because we lack information on the amount of H_2 in these systems. Instead we observe a soft upper limit to the H I surface density of $\sim 10 M_{\odot} \text{pc}^{-2}$ at our resolution of $15''$ (the ‘saturation’ discussed by Bigiel et al. 2008). Figure 13 shows that this pile-up at the saturation extends into the outer disks of dwarf galaxies, though the SFR for $\Sigma_{\text{HI}} \sim 10 M_{\odot} \text{pc}^{-2}$ outside r_{25} is lower than for the same gas inside r_{25} , on average. Unless H_2 represents the majority of the ISM by several times in dwarf galaxies, it seems safe to conclude that as in spirals star formation is more efficient inside the optical disks of dwarf galaxies than at large radii.

Finally, in Figure 14, we look at how the SFE varies as a function of galactocentric radius from 0 to $2 \times r_{25}$. We plot our data at $> r_{25}$ (right of the vertical dashed

line) and measurements by Leroy et al. (2008) inside r_{25} (their Figure 1); we also indicate their fits to the SFE as a function of radius for each sample. As in the case of the SFR vs. gas plot (Figure 13), some discontinuity reflecting the change in methodology is seen around r_{25} (we illustrate the effects of neglecting internal extinction within r_{25} by the black set of contours, which show an extension of the red filled contour of the outer disk data towards smaller radii). Our approach here is not appropriate to investigating the detailed behavior around r_{25} , nor is this our goal; we wish to broadly compare the inner and outer disk regimes.

Again, we see a distinct contrast between the inner and outer disk. The SFEs overall are lower, the scatter in SFE appears larger, and although the first few points in both samples are approximately consistent with the decline measured by Leroy et al. (2008), the overall decline in SFE with radius across the range $1\text{--}2 \times r_{25}$ is markedly more shallow than between 0 and $1 \times r_{25}$.

4. DISCUSSION

4.1. Broad Structure of Star Formation In Outer Disks

Our most basic conclusion is that star formation in outer disks is extremely inefficient compared to star formation inside the optical disks. H I depletion times for most of our data are $\sim 10^{11}$ yr and it is rare to find regions with local depletion times $\lesssim 10^{10}$ yr. These values agree with previous measurements near r_{25} and observations of low surface brightness galaxies (Wyder et al. 2009). Thus present day star formation requires many

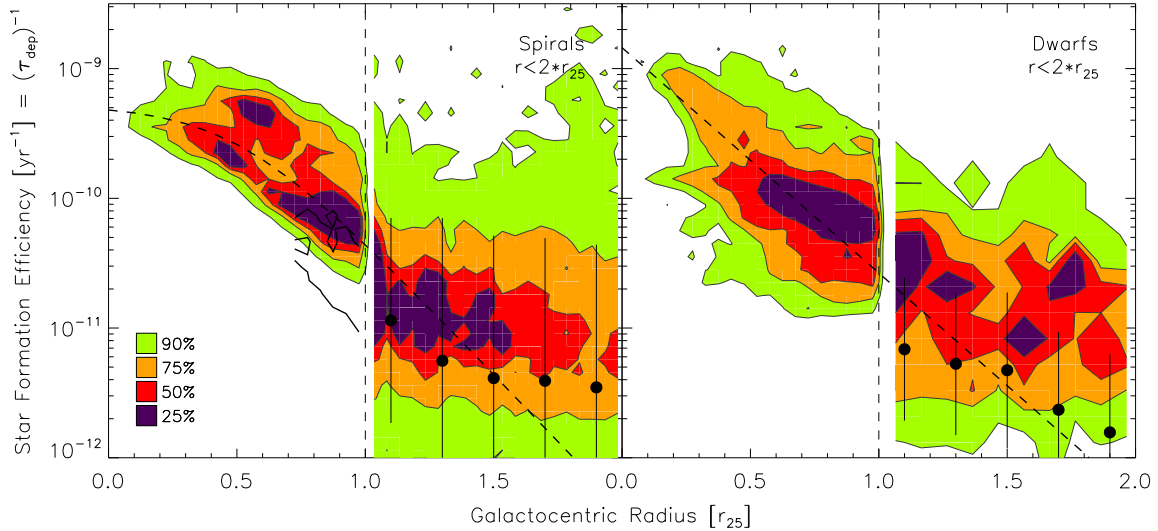


FIG. 14.— SFE (i.e., SFR/gas or FUV/HI) as a function of galactocentric radius from 0 to $2 \times r_{25}$ in spiral (left) and dwarf (right) galaxies. The vertical dashed line indicates r_{25} . Contours and black filled circles right of this line are as in Figure 9. Data inside r_{25} are from Leroy et al. (2008) and are derived accounting for internal extinction and the presence of molecular gas (meaning that some discontinuity at r_{25} may be expected). We illustrate the effects of neglecting these two factors by the black set of contours, which show an extension of the outer disk data (the red contour) towards smaller radii. The dashed lines show fits to the SFE inside r_{25} from Leroy et al. (2008). The outer disk data are roughly consistent with these trends inside $\sim 1.5 r_{25}$ but at large radii the decline in the SFE is more shallow than it is inside the optical disk.

Hubble times ($\sim 10^{10}$ yr) to devour the existing gas reservoir. Another way to look at this is the low integrated SFR of outer galaxy disks: on average, outer disks contribute only about 10% to the total SFR of a galaxy. The relative lack of importance of *in situ* star formation means that the massive extended gas distributions observed in many nearby galaxies can be long-lived and may be viewed as a potential source of fuel for inner disk star formation. The short depletion times in inner disks ($\sim 2 \times 10^9$ yr, Bigiel et al. 2008; Leroy et al. 2008) imply that such a source is required (Shlosman, Frank & Begelman 1989; Blitz 1996; Bauermeister et al. 2009), though the presence and importance of radial gas flows are still debated (e.g., Vollmer & Beckert 2003; Wong et al. 2004; Peek 2009).

Our second simple conclusion is that both H I column and FUV intensity decline systematically at large radii. For H I, this represents a contrast with the inner disk, where the azimuthally averaged H I surface density tends to be flat or even increase with increasing radius. As a result, outer disks are home to column densities seldom found inside the optical radius; in the regime we study in spirals, column densities $< 3 M_{\odot} \text{ pc}^{-2}$ account for the majority of data. For FUV, the decline that we observe outside r_{25} appears approximately consistent with the decline in SFR inferred from combined IR and UV profiles inside r_{25} (Leroy et al. 2008). The rate of decline in H I and FUV intensity for a given galaxy appears to be correlated but not identical; parameterizing the decline with exponential scale lengths, we find the FUV intensity to decline with a scale length approximately half that of the H I. With the SFR declining faster than the gas reservoir, star formation becomes less efficient with increasing radius, though this decline is actually milder than that observed inside r_{25} .

Despite the mismatch in scale lengths, we find a fairly

good overall relationship between H I and FUV (measured via direct scatter plot or rank correlation). This is surprising given the extremely poor correlation between H I and SFR (traced mainly by IR emission) found inside star-forming disks (Wong & Blitz 2002; Kennicutt et al. 2007; Leroy et al. 2008; Bigiel et al. 2008) and gives a strong hint that different physics governs the formation of star-forming clouds at large radii. This agrees qualitatively with the results of Hunter et al. (2010), who found that the integrated HI-richness of dwarf galaxies appears related to outer disk star formation in the sense that HI-poor dwarfs preferentially show suppressed star formation.

4.2. Star Formation Thresholds

Although we do find the SFE to depend on both gas column and radius, we do not find clear evidence for a threshold in either quantity. This agrees with numerous recent studies that have failed to detect such a feature using UV data (e.g., Boissier et al. 2007; Thilker et al. 2005; Hunter et al. 2010; Gil de Paz et al. 2005, 2007b), but is in contrast to the radial cutoffs found in H α emission (e.g., Kennicutt 1989; Martin & Kennicutt 2001). The main new contribution of our work is to look for the signature of such a feature by plotting the SFE of individual lines of sight as a function of H I column density. Doing so, we observe a continuous dependence of SFE on H I column with large scatter rather than an abrupt step at a given H I column density.

What does the lack of a step function in FUV/H I as a function of H I mean? Our angular resolution ($15''$) translates to ~ 750 pc for a typical spiral in our sample ($d \sim 10$ Mpc). A reductionist view of our observations would imply that if there is a critical column density that must be achieved on these scales in order for star formation to occur, then this column density is not maintained over the same timescales and area as the FUV emission

from the young stars that result. Our best estimate is that this is not due to internal extinction or unaccounted H_2 , though in both cases this represents an assumption. It may be a timescale effect, with FUV emission surviving its parent gas. FUV emission at low but significant levels may be found from stellar populations as old as 100 Myr, during which a population with a 10 km s^{-1} dispersion (a plausible dispersion for young stars and roughly the observed dispersion in the gas) might move $\sim 1 \text{ kpc}$. This would allow FUV emission from one resolution element in our line of sight analysis to diffuse to nearby regions and the gas distribution to evolve significantly.

Another explanation is that star formation has only a stochastic relation to kiloparsec scale conditions. In the inner parts of galaxies, star forming clouds are $\sim 50 \text{ pc}$ in size, a factor of 10–20 times smaller than one of our resolution elements. A similar contrast holds in terms of gas mass: even at a relatively modest $\Sigma_{\text{HI}} \approx 1 \text{ M}_\odot \text{ pc}^{-2}$, one of our resolution elements contains $\sim 5 \times 10^5 \text{ M}_\odot$ of H I. This is enough material to make roughly 10 low-mass star-forming regions the mass of the Taurus molecular complex — perhaps a reasonable analog to outer disk star forming regions given the low local SFRs and sparsity of high mass stars. Detailed GALEX studies of outer disks support this picture, finding star formation to be patchy, composed of locally confined ‘FUV knots’ (Gil de Paz et al. 2007a; Thilker et al. 2007) that may match theoretical expectations for this regime (e.g., Elmegreen & Hunter 2006).

An even simpler explanation can be obtained by realizing that local conditions clearly influence the amount and efficiency of star formation in systematic, measurable ways. However, the convolution of a turbulent ISM, random sampling of star-forming clouds along their evolutionary sequence, and the sensitivity of star formation tracers to a range of stellar ages means that star formation ‘thresholds’ will always be observed as continuous trends. The physics discussed by Schaye (2004), Elmegreen & Parravano (1994), and Kennicutt (1989) may drive the trends that we observe, but we expect it is unlikely that any proposed threshold will yield a clear step function on kpc scales (and measurements on much smaller scales risk returning the trivial result that stars form in dense, bound clouds rather than assess where stars can and cannot form on galactic scales).

4.3. *What Regulates Star Formation In Outer Disks?*

We have seen outer disks to be distinct from the inner parts of spirals in several ways: SFEs are low, the gradient in SFE with radius is comparatively weak, and there is a clear spatial correlation between H I and SFE. We have also found the outer disks of dwarf and spiral galaxies to be similar in many ways. All of these, we argue, point to H I column as the regulating quantity for star formation in outer disks. There are two natural reasons for this: first, H I represents the ultimate fuel for star formation and unlike in inner galaxy disks the availability of H I varies dramatically across outer galaxy disks. Second, inasmuch as the outer parts of galaxies are actually organized into disks, the H I column will usually represent the dominant (baryonic) mass component, meaning that the *volume* density of gas (which depends critically on the stellar surface density inside r_{25}) depends mostly on Σ_{HI} . Typical rank correlation coeffi-

cients across the outer disks of our galaxy sample show a comparable degree of local correlation ($r \approx 0.4$) between the SFE and H I column and between SFE and radius. This can be (at least partly) understood as both quantities are strongly anti-correlated (i.e., are not independent; compare Figure 2). The correlation coefficient between SFE and Toomre-Q ($r \lesssim 0.1$) implies little or no local correlation between these quantities.

To first order a line of sight with a given H I column appears to form stars in a way that is largely independent of whether it lies in the outer disk of a dwarf or spiral galaxy. There are second order differences that point to the importance of other factors, however. The most straightforward of these is the large scatter in Σ_{SFR} at a given H I column in spirals. Our estimate of the intrinsic scatter in Σ_{SFR} near $\Sigma_{\text{HI}} \sim 1 \text{ M}_\odot \text{ pc}^{-2}$ is $\approx 1 \text{ dex}$. Some of this might be expected from the low values involved: the median SFR for the lowest bins corresponds to forming only a few hundred solar masses every 100 Myr. However, over the same range dwarf galaxies show significantly less scatter; with such a small sample of dwarfs it is hard to know whether the difference is significant, but if it is then an easy interpretation is that the larger scatter in spirals reflects the wider range of environments found there (e.g., our sample includes spirals with strong metallicity gradients like M 101 and such with shallow gradients like M 51 and M 83).

What can we say about the efficiency of the regulation of star formation in outer disks? In the inner parts of galaxies stars form out of molecular clouds with a depletion time of a few times 10^9 yr . Across both dwarfs and spirals we find H I depletion times in outer galaxies two orders of magnitude higher, $\sim 10^{11} \text{ yr}$. If an outer disk star-forming cloud resembles its inner disk counterpart (a big assumption), then only $\sim 1\%$ of the gas in outer galaxy disks is actually in star forming clouds (or about $\sim 5,000 \text{ M}_\odot$ in one of our typical resolution elements). Similarly, if we take the orbital time to be $\sim 0.5 \text{ Gyr}$ (roughly appropriate for the Milky Way around r_{25}) then only $\sim 0.1\%$ of the gas is converted into stars per orbital time, two orders of magnitude below the galaxy-averaged value of Kennicutt (1998). Assuming a typical scale height of $\sim 500 \text{ pc}$, average volume densities in the outer disks will be $\sim 0.1 \text{ cm}^{-3}$, implying a disk free-fall time of $\sim 10^8 \text{ yr}$. Krumholz & McKee (2005) and Krumholz & Thompson (2007) argued that star-forming structures on many scales convert $\sim 1\%$ of their gas to stars per free-fall time. Outer galaxy disks apparently have about a tenth that efficiency on average.

4.4. *Towards a Complete Star Formation ‘Law’*

Finally, we comment on the apparently ‘baroque’ nature of the ‘star formation law’ plot seen in Figure 13. The plot shows a complex star formation law, with at least three (somewhat) distinct regimes observed — outer disks, the H I-dominated parts of inner disks, and the H_2 -dominated parts of inner disks. Another regime is well-established: starburst galaxies are known to have a steeper power law index than the H_2 -dominated parts of spirals in Figure 13, so that the plot should ‘turn up’ again at $\Sigma_{\text{gas}} \approx 100 \text{ M}_\odot \text{ pc}^{-2}$ (compare discussion in Bigiel et al. 2008). Different parts of the ‘S-shape’ (a ‘W-shape’ with the starbursts) represent physically truly distinct regimes. We argue that this kind of behavior —

a series of regime-dependent relations that combine into a complex distribution — is actually exactly what one would expect if the ability to form stars or star-forming clouds has a significant environmental dependence and multiple environments are combined on a single plot.

5. SUMMARY

Using high resolution ($\sim 15''$), sensitive, wide field-of-view data we have studied the relationship between H I gas and star formation traced by UV light in the outer disks ($1-2 \times r_{25}$) of 17 spiral and 5 dwarf galaxies. We expect that H I dominates the ISM in this regime and that FUV reflects the distribution of recently formed stars without large biases due to internal extinction.

We find that:

1. Despite widespread star formation the gas depletion time is very low in outer galaxy disks, almost always longer than 10^{10} yr and typically $\sim 10^{11}$ yr. Star formation at the present rate will thus not appreciably deplete the gas supply in the outer disks over timescales shorter than many Hubble times.
2. FUV emission in outer disks declines approximately exponentially with a scale length comparable to that found for star formation in the inner parts of galaxies. H I gas also usually shows a systematic decline, but a shallower one than the FUV. The H I scale length that we derive for outer disks is typically twice the FUV scale length. As a result, the ratio of H I to FUV and thus the gas (H I) depletion time, increases with radius. However, this increase is weaker than that observed inside r_{25} , so that overall the depletion time as a function of radius becomes ‘flatter’ as one moves out in a galaxy.
3. Unlike in the inner parts of galaxies, there is a fairly clear relationship between star formation and H I in outer galaxy disks. This is clearest near the optical radius, where the H I and FUV are strongly correlated (rank correlation ~ 0.7). Extinction and the presence of H₂ wash out this correlation at radii $< r_{25}$ and the strength of the correlation also decreases with increasing radius ($r > r_{25}$), perhaps due to the increasing scatter/stochasticity in star formation at these radii. A fit of depletion time vs. Σ_{HI} to binned outer disk data yields $\tau_{\text{Dep}} \propto (\Sigma_{\text{HI}})^{0.7}$, or $\Sigma_{\text{SFR}} \propto (\Sigma_{\text{HI}})^{1.7}$ for both spiral and dwarf galaxies.
4. At a given H I column density, one finds similar FUV intensities in the outer disks of dwarf and spiral galaxies. The main difference between the two samples is the distribution of H I column densities at large radius. Dwarf galaxies tend to have (relatively) more high-column H I than spirals. In both samples, low columns become more common with increasing radius.
5. Examining the relationship for individual lines of sight, we do not find clear evidence for a step-function type star formation threshold in either radius or H I column, though the SFE is a weak function of both quantities.

6. The relationship between Σ_{SFR} and Σ_{gas} for individual lines of sight extends that measured by Bigiel et al. (2008) into a new regime of low Σ_{SFR} and low Σ_{gas} more or less continuously. In this regime, a line of fixed $\tau_{\text{Dep}} \sim 10^{10}$ yr forms an approximate upper envelope to the distribution. Lines of sight with high H I columns ($\Sigma_{\text{gas}} \approx 3-10 M_{\odot} \text{ pc}^{-2}$) but little or no FUV emission are rare. These conclusions apply to both dwarf and spiral galaxies.

We thank the GALEX NGS team for creating and making available their outstanding dataset. F.B. acknowledges support from NSF grant AST-0838258 and earlier support from the Deutsche Forschungsgemeinschaft (DFG) Priority Program 1177. Support for A.L. was provided by NASA through Hubble Fellowship grant HST-HF-51258.01-A awarded by the Space Telescope Science Institute, which is operated by the Association of Universities for Research in Astronomy, Inc., for NASA, under contract NAS 5-26555. The work of W.J.G.d.B. is based upon research supported by the South African Research Chairs Initiative of the Department of Science and Technology and National Research Foundation. We have made use of the Extragalactic Database (NED), which is operated by the Jet Propulsion Laboratory, California Institute of Technology, under contract with the National Aeronautics and Space Administration. This research has made use of NASA’s Astrophysics Data System (ADS).

REFERENCES

- Bauermeister, A., Blitz, L., & Ma, C.-P. 2009, ApJ, submitted, arXiv:0909.3840
- Bigiel, F., Leroy, A., Walter, F., Brinks, E., de Blok, W. J. G., Madore, B., & Thornley, M. D. 2008, AJ, 136, 2846
- Bigiel, F., et al. 2010, ApJ, in press
- Blitz, L. in 25 Years of Millimeter Wave Spectroscopy, ed. W. B. Latter, S. J. E. Radford, P. R. Jewell, J. G. Mangum, & J. Bally (Dordrecht: Kluwer), 11
- Bohlin, R. C., Savage, B. D., & Drake, J. F. 1978, ApJ, 224, 132
- Boissier, S., Prantzos, N., Boselli, A., & Gavazzi, G. 2003, MNRAS, 346, 1215
- Boissier, S., et al. 2007, ApJS, 173, 524
- Braine, J., & Herpin, F. 2004, Nature, 432, 369
- Braine, J., Ferguson, A. M. N., Bertoldi, F., & Wilson, C. D. 2007, ApJ, 669, L73
- Bresolin, F., Ryan-Weber, E., Kennicutt, R. C., & Goddard, Q. 2009, ApJ, 695, 580
- Bush, S. J., Cox, T. J., Hernquist, L., Thilker, D., & Younger, J. D. 2008, ApJ, 683, L13
- Bush, S. J., Cox, T. J., Hayward, C. C., Thilker, D., Hernquist, L., & Besla, G. 2010, ApJ, 713, 780
- Calzetti, D., et al. 2007, ApJ, 666, 870
- Christlein, D., & Zaritsky, D. 2008, ApJ, 680, 1053
- Cuillandre, J.-C., Lequeux, J., Allen, R. J., Mellier, Y., & Bertin, E. 2001, ApJ, 554, 190
- de Blok, W. J. G., & Walter, F. 2006, AJ, 131, 363
- de Blok, W. J. G., Walter, F., Brinks, E., Trachternach, C., Oh, S.-H., & Kennicutt, R. C. 2008, AJ, 136, 2648
- de Blok, W. J. G., & Walter, F. 2003, MNRAS, 341, L39
- Donas, J., Milliard, B., Laget, M., & Deharveng, J. M. 1981, A&A, 97, L7
- Dong, H., Calzetti, D., Regan, M., Thilker, D., Bianchi, L., Meurer, G. R., & Walter, F. 2008, AJ, 136, 479
- Elmegreen, B. G., & Parravano, A. 1994, ApJ, 435, L121
- Elmegreen, B. G., & Hunter, D. A. 2006, ApJ, 636, 712
- Ferguson, A. M. N., Wyse, R. F. G., Gallagher, J. S., & Hunter, D. A. 1998, ApJ, 506, L19
- Gardan, E., Braine, J., Schuster, K. F., Brouillet, N., & Sievers, A. 2007, A&A, 473, 91
- Gil de Paz, A., et al. 2005, ApJ, 627, L29
- Gil de Paz, A., et al. 2007, ApJS, 173, 185
- Gil de Paz, A., et al. 2007, ApJ, 661, 115
- Goddard, Q. E., Kennicutt, R. C., & Ryan-Weber, E. V. 2010, MNRAS, 644
- Herbert-Fort, S., Zaritsky, D., Christlein, D., & Kannappan, S. J. 2010, ApJ, 715, 902
- Hunter, D. A., Elmegreen, B. G., & Ludka, B. C. 2010, AJ, 139, 447
- Jog, C. J., & Solomon, P. M. 1984, ApJ, 276, 127
- Kennicutt, R. C., Jr. 1989, ApJ, 344, 685
- Kennicutt, R. C., Jr. 1998, ApJ, 498, 541
- Kennicutt, R. C., Jr., et al. 2007, ApJ, 671, 333
- Krumholz, M. R. & McKee, C. F. 2005, ApJ, 630, 250
- Krumholz, M. R. & Thompson, T. A. 2007, ApJ, 669, 289
- Leitherer, C., et al. 1999, ApJS, 123, 3
- Lelièvre, M., & Roy, J.-R. 2000, AJ, 120, 1306
- Leroy, A. K., Walter, F., Brinks, E., Bigiel, F., de Blok, W. J. G., Madore, B., & Thornley, M. D. 2008, AJ, 136, 2782
- Leroy, A. K., et al. 2009, AJ, 137, 4670
- Li, Y., Mac Low, M.-M., & Klessen, R. S. 2005, ApJ, 626, 823
- Martin, C. L., & Kennicutt, R. C., Jr. 2001, ApJ, 555, 301
- Morrissey, P., et al. 2005, ApJ, 619, L7
- Peek, J. E. G. 2009, ApJ, 698, 1429
- Pohlen, M., & Trujillo, I. 2006, A&A, 454, 759
- Popescu, C. C., & Tuffs, R. J. 2003, A&A, 410, L21
- Press, W. H., Teukolsky, S. A., Vetterling, W. T., & Flannery, B. P., *Numerical Recipes in FORTRAN. The Art of Scientific Computing*, Cambridge University Press, 1992, 2nd ed.
- Rafikov, R. R. 2001, MNRAS, 323, 445
- Salim, S., et al. 2007, ApJS, 173, 267
- Schaye, J. 2004, ApJ, 609, 667
- Schlegel, D. J., Finkbeiner, D. P. & Davis, M. 1998, ApJ, 500, 525
- Shlosman, I., Frank, J. & Begelman, M. C. 1989, Nature, 338, 45
- Tamburro, D., Rix, H.-W., Leroy, A. K., Low, M.-M. M., Walter, F., Kennicutt, R. C., Brinks, E., & de Blok, W. J. G. 2009, AJ, 137, 4424
- Toomre, A. 1964, ApJ, 139, 1217
- Thilker, D. A., et al. 2005, ApJ, 619, L79
- Thilker, D. A., et al. 2007, ApJS, 173, 538
- Thilker, D. A., et al. 2009, Nature, 457, 990
- Vollmer, B., & Beckert, T. 2003, A&A, 404, 21
- Walter, F., Brinks, E., de Blok, W. J. G., Bigiel, F., Kennicutt, R. C., Thornley, M. D., & Leroy, A. 2008, AJ, 136, 2563
- Werk, J. K., et al. 2010, AJ, 139, 279
- Wong, T. & Blitz, L. 2002, ApJ, 569, 157
- Wong, T., Blitz, L. & Bosma, A. 2004, ApJ, 605, 183
- Wyder, T. K., et al. 2007, ApJS, 173, 293
- Wyder, T. K., et al. 2009, ApJ, 696, 1834
- Yang, C.-C., Gruendl, R. A., Chu, Y.-H., Mac Low, M.-M., & Fukui, Y. 2007, ApJ, 671, 374
- Zaritsky, D. 1994, AJ, 108, 1619
- Zaritsky, D., & Christlein, D. 2007, AJ, 134, 135